Tesi doctoral presentada per En/Na

Marc PERA TITUS

amb el títol

"Preparation, characterization and modeling of zeolite NaA membranes for the pervaporation dehydration of alcohol mixtures"

per a l'obtenció del títol de Doctor/a en

QUÍMICA

Barcelona, 29 de maig del 2006

Facultat de Química
Departament d'Enginyeria Química

UNIVERSITAT DE BARCELONA

I.1. INTRODUCTION TO MEMBRANE SEPARATION

A membrane can be defined as a semipermeable active or passive barrier which, under a certain driving force, allows preferential passage of one or more species or compounds (molecules, particles or polymers) of a gaseous and/or liquid mixture or solution. The stream rejected by a membrane is called ***retentate***, while that passing through the membrane is termed ***permeate***. The key parameters in the operation of a membrane are the flux, permeance or permeability[1] and the selectivity or separation factor, which provide information, respectively, concerning the mass transfer across the barrier and its ability to separate one or more species of a mixture. The flux has units of [mass area^{-1} time^{-1}], whose value is calculated by dividing the permeation flux rate by the membrane area. The permeance, with units of [mass area^{-1} time^{-1} pressure^{-1}], is defined as the flux divided by the pressure difference across the membrane. Finally, the permeability is calculated by multiplying the permeance by the thickness of a membrane layer [mass length^{-1} time^{-1} pressure^{-1}]. The selectivity is defined as the ratio of the molar fractions of two species in the permeate to that in the retentate in the membrane module. Multi-component selectivity depends not only on the thermodynamic and mass transfer properties of the membrane/fluid mixture, but also on the configuration of the permeation module and the flux conditions of the permeation measurement. As a general rule, membranes with high permeances or permeabilities usually show low selectivities, and the opposite.

The driving force across a membrane can exist either as a pressure, concentration, or voltage difference. According to the driving force of the separation and to the physical size of the separated species, membrane processes can be broadly classified as: microfiltration (MF), ultrafiltration (UF), nanofiltration (NF), reverse osmosis (RO), dialysis (D), electrodialysis (ED), pervaporation (PV) and gas separation (GS) (see Table I.1). Since the 60s, the membrane market has been dominated by polymeric membranes, which after many years of research and development enjoy applications ranging from desalination of sea and brackish waters, food and beverage processing, separation of azeotropic and close-boiling liquid mixtures, gas separation, and hemodialysis. The membrane and module sales in 1998 were estimated at more than US$ 4.4 billion worldwide (*Nunes and Peinemann, 2001*), shared by the aforementioned applications. MF covers most of the practical applications with about 2/3 of the market volume (*Caro et al., 2000*). Although the membrane research has focused mostly on polymeric membranes, one of the major targets remained so far is the development of microporous inorganic membranes.

[1] The term permeance is usually used in the field of gas separation, while the term permeability is preferred for separations in liquid phase.

Table I.1: Membrane separation processes (*Feng and Huang, 1997; Nunes and Peinemann, 2001*)

PROCESS	*DRIVING FORCE*	*SEPARATED SIZE*	*EXAMPLES OFAPPLICATION*
Microfiltration (MF)	Pressure difference (10 - 500 kPa)	0.1 – 10 μm	▪ Clarification and sterilization of liquids (pharmaceutical industry), fruit juice, wine,…
Nanofiltration (NF)	Pressure difference (0.1 - 1 MPa)	5 – 10 nm	▪ Separation of salts and microsolutes from solutions (water softening)
Ultrafiltration (UF)	Pressure difference (0.1 - 1 MPa)	1 – 5 nm	▪ Separation of macromolecular solutions (recover of paints in motoring industry)
Reverse osmosis (RO)	Pressure difference (2 - 10 MPa)	< 5 nm	▪ Separation of salts and microsolutes from solutions (desalinization of seawater)
Dialysis (D)	Concentration difference	< 5 nm	▪ Separation of salts and microsolutes from macromolecular solutions (hemodialysis in renal patients)
Electrodialysis (ED)	Voltage	< 5 nm	▪ Desalinization of ionic solutions (seawater) ▪ Production of NaCl
Pervaporation (PV)	Partial pressure difference	< 1 nm	▪ Separation of azeotropic and close-boiling mixtures
Vapor permeation (VP)	Partial pressure difference	< 1 nm	▪ Separation of azeotropic and close-boiling mixtures
Gas separation (GS)	Pressure difference (0.1 – 10 MPa)	< 1 nm	▪ Environmental control ▪ Separation of inorganic gases (e.g., H_2 / N_2) ▪ Separation of organic gases (e.g., hydrocarbons)

I.2. INTRODUCTION TO INORGANIC MEMBRANES

In recent years there has been an increasing interest in the production of inorganic membranes for processes in which temperature, pressure or the chemical environment (e.g., pH and chlorine) prevent the use of polymeric membranes. The development of inorganic membranes for MF and UF purposes began in the early 80s, and by now they are commercially available. According to *Caro et al. (2000)*, the mean annual growth rate of inorganic membranes is about 30% and their production reaches ca. 15% of the present membrane market volume. The general advantages and disadvantages of inorganic membranes are compared in Table I.2. In addition to their improved thermal, mechanical and chemical stability, inorganic membranes show specific advantages such as the possibility to be sterilized and the biocompatibility displayed by some inorganic membrane materials.

In fact, although the potential applications of inorganic materials such as platinum and porous glass-type membranes were evident in the beginning of the last century, the studies

concerning the field of inorganic membranes have not been extended until recent times, as new demands of inorganic membranes in fuel cells and in catalytic membrane reactors are increasingly required. The foreseeable development of supported zeolite membranes and stabilized sol-gel membranes in multichannel tube or ceramic hollow fiber is envisaged to improve the competitiveness of inorganic microporous membranes for NF, PV and gas/vapor separations (*Caro et al., 2000*). Several unique permeation and separation properties have been reported on microporous inorganic membranes.

Table I.2: Advantages and drawbacks of inorganic membranes in comparison with polymeric membranes (*Caro et al., 2000*)

Reasons for inorganic membranes	*Reasons against inorganic membranes*
Long-term stability at high temperatures Resistance to harsh environments Resistance to high pressure drops Inertness to microbiological degradation	High capital costs Brittleness Low membrane surface per module volume Difficulty in achieving high selectivities in large scale membranes
Easy cleanability after fouling	Generally low permeability of the highly selective (dense) membranes at medium temperatures
Easy catalytic activation	Difficult membrane-to-module sealing at high temperatures

I.2.1. Classification of inorganic membranes

A wide spectrum of inorganic membranes prepared from different materials and methods can be found in the literature. Inorganic membranes can be classified as ***symmetric*** or ***isotropic***, and ***asymmetric*** or ***anisotropic*** depending on whether they are constituted by a pure phase (self-supported membranes) or they are synthesized onto a support of different nature (supported membranes).

- **Symmetric or isotropic membranes**: The membranes can be directly prepared, without a support, or onto a provisional support, usually PTFE or stainless steel, which is removed after the synthesis. There are not many applications of these membranes at present time because of their disadvantages related to their small dimensions, the heterogeneity of the layer and the low mechanical resistance.

- **Asymmetric or anisotropic membranes**: The membranes are synthesized onto a flat/tubular polymeric or inorganic MF or UF support (metal, alumina,…). More applications of these membranes compared to self-supported have been reported, especially onto inorganic supports, because of their better properties related to their

thermal, chemical, mechanical stability than polymeric supports. The thickness of the layer varies from a few ten-nanometers (*thin layers*) to a few microns (*thick layers*).

According to their structural characteristics, which have significant impact on their performance, both symmetric and asymmetric inorganic membranes can be divided into three main categories: *dense*, *porous* and *composite* (combination of dense-dense or dense-porous materials) (*Hsieh, 1996*) (see Table I.3).

Table I.3: Classification and characteristics of inorganic membranes (*Hsieh, 1996*)

Type of membrane		*Material of the membrane*	*Driving force*	*Selectivity*	*Permeation*	*Features*
DENSE		Metal (Pd, Pd/Ru, Ag, Ni, Au, Rh,…)	Solution/ Diffusion	Selective H_2(Pd) O_2(Ag)	Low/ moderate	Without pores
		Solid electrolytes (Zr, Tl, Ce, Y,... oxides)		Selective H_2, O_2 as H^+, O^{2-}		
		Metal, ceramic with immobilized liquids	Chemical reaction	Selective O_2, NH_3		
POROUS	**Macro (>50 nm)**	• Metallic oxides (Al, Zr, Ti, Mg, Cr, Sn,…) • Zeolites • C fiber or glass • Metals (Pd)	Pore Diffusion	Non selective	High	Porous thin layer
	Meso (2-50 nm)			Can be selective	Moderate/ High	
	Micro (<2 nm			Selective	Moderate	
COMPOSITE		• Metal-glass • Metal-ceramic • Metal-metal (metal = Pd, Ag, Pd/Ag,…)	Solution/ Diffusion Diffusion	Selective	Moderate	Combination of the former

I.2.1.1. Dense membranes

Dense membranes are free of discrete, well-defined pores or voids and their effectiveness depends on their materials, the species to be separated and their interactions with the membrane. Historically, there are two major types of dense inorganic membranes that have been studied and developed extensively: ***metal*** and ***solid electrolyte membranes***, especially for H_2 and O_2 gas separations. Among metal membranes, those made of Pd have been widely studied (e.g., *Jayaraman and Lin, 1995; McCool et al., 1999*). More recently, new

applications of ceramic membranes with immobilized liquids have been also developed. The selectivity of these membranes can be extremely high, but they offer the important shortcoming of very low gas permeances.

I.2.1.2. Porous membranes

Porous inorganic membranes are constituted by a discrete and well-defined pore size distribution. In contrast to dense inorganic membranes, their rate of advances towards industrial-scale application has been rapid in recent years. The first applications of porous inorganic membranes are encountered in the beginning of the 20^{th} century in the field of MF and, in the decade of 40s, microporous Vycor-type glass membranes became available. However, gas separation for uranium enrichment in the field of nuclear technology constitutes the first large-scale application of this kind of membranes (concentration of ^{235}U isotope from natural uranium) (*Feng and Huang, 1997*). Since then, new microporous inorganic materials have been surveyed for separation purposes, which fall into two categories according to their structural characteristics: crystalline (mainly zeolites) and amorphous (mainly SiO_2 and active carbon) materials.

Porous inorganic membranes frequently comprise a thin and continuous layer of porous material deposited onto a ceramic or stainless steel support of higher pore size which provides the required mechanical resistance (asymmetric membrane), which are usually prepared by means of the sol-gel method (*Brinker and Scherer, 1990; de Vos and Verweij, 1998*). Compared to dense membranes, they usually offer higher permeabilities. In general terms, as the pore size of the membrane increases, the permeability of the membrane also does so, although the membrane becomes less selective.

I.2.2. Mass transfer mechanisms in inorganic membranes

The mass transfer mechanisms in a membrane indicate how a set of molecules of one or several species are transferred along the pores of a membrane layer. The mass transfer across a membrane depends on the pressure and temperature conditions, as well as on the pore size of the membrane and on the properties of the permeating molecules (molecular weight, kinetic diameter and heat of adsorption). Figure I.1 summarizes the mechanisms that can take place in an inorganic membrane.

a. ***Viscous or Poiseuille flux***: This mechanism is based on a laminar non-selective mass transfer along the pores of the membrane due to the action of a pressure gradient between its both sides. It takes place in porous membranes whose pore size is higher

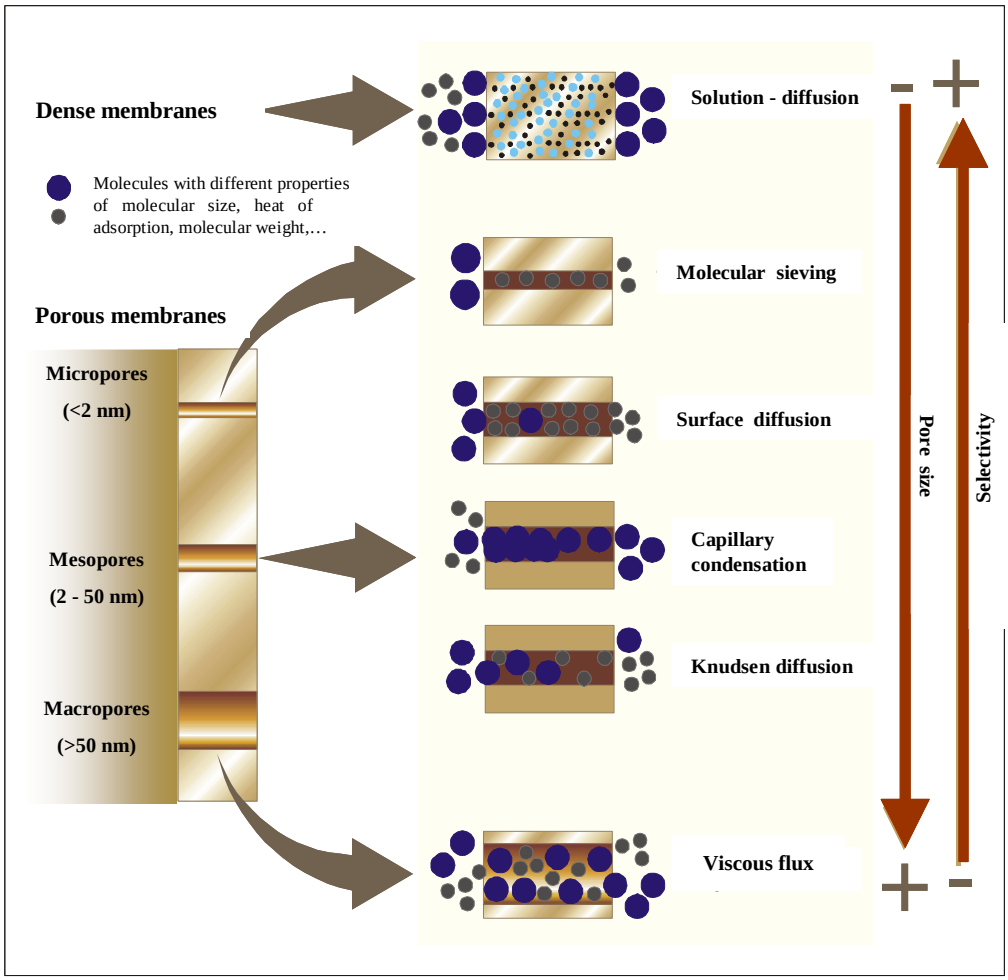

Figure I.1: Mass transfer mechanisms in a membrane (*Hsieh et al., 1996*)

than the mean-free path (λ) of the permeating molecules, which is defined in the *Kinetic Theory of Gases* as the mean distance that a molecule runs between two consecutive collisions, and which depends on the pressure and temperature conditions. For ideal gases, it can be calculated by Eq. I.1

$$\lambda = \frac{1}{\sqrt{2\pi d_m^2}} \frac{RT}{PN_A}, \qquad \text{(Eq. I.1)}$$

where $\mathbf{d_m}$ is the kinetic diameter of the molecules [m] and $\mathbf{N_A}$ is the Avogadro Number (6.023×10^{23} mol^{-1}).

b. ***Knudsen diffusion***: In this case, the pore size of the membrane is lower than the mean-free path of the permeating molecules. As a result, the frequency of collisions with the

pore walls is higher than that of intermolecular collisions. The selectivity is usually low, except for permeating molecules with very different molecular weights, for instance in the dehydrogenation of hydrocarbons of high molecular weight. The selectivity towards the separation of two different molecules **i** and **j** ($d_{m,i} < d_{m,j}$) is defined by Eq. I.2

$$\alpha_{i,j} = \sqrt{\frac{M_j}{M_i}} > 1, \qquad \text{(Eq. I.2)}$$

where M_i and M_j are the molecular weights of the species **i** and **j**, respectively. At intermediate pressures, both viscous and Knudsen fluxes can take place simultaneously.

c. ***Surface diffusion***: It can appear when a membrane permeates adsorbed species onto the porous material by jumping from one adsorption site to another across the membrane. If the adsorption is too strong, surface diffusion becomes deterred, while if it is too weak, it does not contribute much to the overall mass transfer. Surface diffusion and viscous flux usually take place simultaneously, but the former plays a more relevant role at lower temperatures (<500 K), because the stronger adsorbed molecules tend to block totally or partially the entry of other molecules to the pores, thus becoming the membrane selective.

d. ***Capillary condensation***: This mechanism occurs in the separation of gaseous mixtures with condensable vapors. As it is predicted by the Kelvin equation (Eq. I.3), one or more vapor species of a mixture can be condensed in the pores of the membrane if they are small enough, although the saturation pressure of the vapor is not reached:

$$\mathrm{Ln}\left(\frac{P_v}{P^o}\right) = -\frac{4\sigma\overline{V}}{d_p RT}, \qquad \text{(Eq. I.3)}$$

where $\mathbf{P_v}$ and $\mathbf{P^o}$ are, respectively, the vapor pressure of a drop of size $\mathbf{d_p}$ [m] and the saturation vapor pressure [Pa]; $\boldsymbol{\sigma}$ is the surface tension [N m^{-1}]; and $\overline{\mathbf{V}}$ is the liquid molar volume [m^3 mol^{-1}]. This mechanism is highly selective, because the diffusion of non-condensable species ideally depends on their retention in the membrane pores.

e. ***Molecular sieve***: It takes place when the mean pore size of the membrane is very small and it can discriminate between two or more species depending on their molecular size. The membrane acts as a sieve that only lets the permeation of species with a molecular size lower than that of the pore.

f. ***Solution-diffusion***: This is the common mechanism for dense inorganic membranes (and classically for polymeric membranes) and it does not usually take place in porous

membranes. The permeating species adsorb onto the surface of the membrane (they are regarded as dissolved), diffuse to the permeate surface and finally desorb.

The presence of a dominant mechanism in the mass transfer process across a membrane depends on its mean pore size, pressure and temperature conditions, and on the properties of the permeating species (molecular weight, molecular size and heat of adsorption). When the membranes are asymmetric, the resistance to mass transfer of the thin layer and that of the support are combined in series, tending the former to control the mass transfer across the membrane. Some parallel mechanisms can also appear when the thin layer shows pore size heterogeneity or defects.

The separation ability of porous membranes is strongly governed by their pore size distribution according to the viscous flux, Knudsen diffusion, molecular sieve and surface diffusion mechanisms (see Figure I.1). In general terms, the two latter mechanisms tend to be dominant as the ratio between the kinetic diameter of the molecules and the mean pore size of the membrane tends to 1 ($d_m/\overline{d}_p \rightarrow 1$), that is for microporous membranes. Otherwise, for meso- and macroporus membranes, their permeation performance is strongly governed by the viscous flux and Knudsen diffusion mechanisms. In light of the relevance of the porous nature in meso- and macroporous membranes and, in particular, of their pore size distribution, the next section is devoted to surveying the most widespread methods for their characterization, together with some more incipient that can be found in the literature.

I.2.3. Characterization of pore size and pore size distributions (PSDs) in meso- and macroporous membranes: an overview

Although meso- and macroporous membranes are traditionally characterized by means of a single mean pore size or molecular weight cut-off value (MWCO [kDa]), the molecular weight of a solute at which 90% separation can be achieved (*Scott, 1995*), these single data do not provide much information concerning neither their separation performance nor structure. In fact, two membranes with the same mean pore size or MWCO value, but with different PSDs, can show quite different separation behavior. The PSD in meso- and macroporous membranes constitutes an essential issue not only for the understanding of their permeating mechanisms and for the prediction of their separation characteristics, but also for the selection and development of suitable synthesis methods. Consequently, considerable efforts have been directed in the past aimed at the elucidation of PSDs in these kind of membranes.

The currently available characterization techniques of meso- and macroporous membranes cover a broad range of physical methods. A detailed and comprehensive survey

about some conventional and more incipient membrane characterization methods is given in Table I.4. In general terms, these characterization methods can be divided into two main groups (*Nakao, 1994; Zhao et al., 2000a*). One the one hand, some methods are related to membrane permeation and rejection performance, which comprise gas-liquid porometry and liquid-liquid displacement methods, mercury porosimetry, permporometry, liquid and gas permeability tests and solute rejection or sieving. On the other hand, other methods are related to the surface morphology of the membranes, including the well-established gas adsorption and desorption method, some microscopy techniques and thermoporometry, and more incipient methods such as ultrasonic frequency-domain reflectometry (UFDR), light transmission, spectroscopic ellipsometry, nuclear magnetic resonance (NMR), small-angle neutron scattering (SANS), electron spin resonance (ESR), and other ones based on some electrokinetic phenomena.

As can be seen in Table I.4, each method is specific for the characterization of a particular pore size range and presents some limitations. Although, since the early works of *Zeman (1992a, 1992b*), electron microscopy (SEM, TEM and FESEM) and Atomic Force Microscopy (AFM, both *contact* and *tapping* modes) have been widely used to visualize the surface morphology of both polymeric and ceramic membranes and to obtain PSDs and porosities from further computerized image analysis, the translation of images into predictions of PSDs and separation performance is not always straightforward. In fact, active pores to permeation cannot be easily distinguished from dead-end pores in mesoporous membranes, thus providing an under- or overestimation of mean pore sizes (*Singh et al., 1998*). Other important shortcomings concerning microscopic techniques are related to their destructive character and to their low representativity.

Other methods that rely on the relationship between pore size and pressure (gas/liquid, liquid/liquid porometry and permporometry) have also been commonly used to characterize PSDs (*Scott, 1995*). While the former two consist of the determination of a PSD from the flux of a gas or liquid through a membrane wetted with another immiscible liquid, the latter is based on the variation of the flux of a wetting gas through a membrane due to a controlled pore blocking by capillary condensation. Problems arise when interpreting data from these techniques on the grounds of the uncertainty in the determination of contact angles as well as pore necking. In addition, porometry techniques also present some technical limitations in the determination of PSDs of UF and NF membranes because of the excessively high pressures that are often required, which might damage the membrane structure. In fact, gas/liquid porometry is usually restricted to the detection of defects such as cracks or pinholes or very large pores as a primary membrane integrity test (bubble point method, ASTM standard – procedures F316-86 and Modified Boiling Point Method) (*Scott, 1995*).

Table I.4: Classification of the available techniques for the determination of PSD in meso- and macroporous membranes.

Group	*Method*	*Fundament*	*Pore size [nm]*	*Characteristics*	*References*
Methods related to permeation or rejection performance	Gas-liquid porometry	Measurement of the pressure required to blow air through a liquid-filled porous membrane (bubble point test: ASTM standard procedures F316-86 and MBPM)	>50	➢ Inappropriate for UF and NF membranes, because very high pressures are required ➢ Difficult quantification of the contribution of gas diffusion	Jakobs and Koros (1997) Mietton-Peuchot et al. (1997) Shao et al. (2004) Shinde et al. (1999)
	Liquid-liquid porometry or displacement	Similar to bubble point method, but a non-wetting liquid is used instead of a gas as a flowing medium	>2	➢ Good accuracy and reproducibility ➢ Non-destructive and fast technique, which only refers to pores open to flux	Calvo et al. (1997, 2004) Gijsberten-Abra. et al. (2004) Lee et al. (1997) Mc Guire et al. (1995)
	Mercury porosimetry	Introduction of mercury (non-wetting liquid) in the pores of the membrane by applying an external pressure to overcome the interfacial tension	>3	➢ Modified version of liquid-liquid displacement technique ➢ Destructive technique ➢ Use of Hg, which is forbidden in many countries	Hernandez et al. (1998) Scott (1995)
	Permporometry	Variation of gas flux through a membrane due to a controlled pore blocking by capillary condensation	>5	➢ Only pores active to permeation are detected	Huang et al. (1996) Nishiyama et al. (2003) Tsuru et al. (2003)
	Liquid and gas flux measurement	Liquid and gas permeabilities are monitored as a function of the pressure drop across the membrane	All	➢ Only rough information concerning the PSD can be obtained ➢ Cheap and easy-to-operate set-up	Scott (1995)
	Solute rejection or sieving	Measurement of the retention of either nonionic or charged solutes of different molecular weight	>2-3	➢ Reflection coefficient is a function of the solute size (e.g., dextrans)	Aimar et al. (1990) Lee et al. (2002) Leypoldt (1987) Singh et al. (1998)

Table I.4 (to be continued)

Group	*Method*	*Fundament*	*Pore size [nm]*	*Characteristics*	*References*
Methods related to surface morphology	Microscopy techniques*: SEM TEM FESEM AFM	Visualization of the top and cross section of a membrane and determination of PSD from further computerized image analysis	>1	➢ Presence of artifacts onto the surface due to sample preparation ➢ High electron beam energy in SEM and TEM may damage the samples ➢ Destructive techniques ➢ No distinction between active and dead end pores	Bowen and Doneva (2000) Bowen et al. (1997) Calvo et al. (1997, 2004) Hernandez et al. (1998) Khayet et al. (2004) Masselin et al. (2001) Pradanos et al. (1996)
	Gas adsorption/desorption	Determination of the PSD from the adsorption or the desorption isotherms	>0.1	➢ No distinction between active and dead end pores	Calvo et al. (1997) Pradanos et al. (1996)
	Thermoporometry	Calorimetric study of the liquid-solid transformation of a capillary condensate that saturates the pores	>2	-	Ishikiriyama et al. (1995) Iza et al. (2000)
	Ultrasonic frequency domain reflectometry (UFDR)	Determination of characteristic acoustic responses from a membrane	260-280**	➢ Non-destructive technique	Ramaswamy et al. (2004)
	Light transmission	Determination of the light transmitivity through a porous membrane filled with a transparent liquid	100-900**	➢ Cheap and easy-to-operate set-up	Youn et al. (1998)
	Spectroscopic ellipso-metry	Variation of the refractive index of during adsorption and desorption of a gas in the porous structure	1-2**	➢ Non-destructive technique adapted to thin film characterization	Bougeois et al. (2003)

Table I.4 (to be continued)

Group	*Method*	*Fundaments*	*Pore size [nm]*	*Characteristics*	*References*
Methods related to surface morphology	Nuclear magnetic resonance (NMR)	Measurement of NMR spin-lattice relaxation times of water molecules condensed in the pores of a membrane Measurement of carrier diffusivity within the pores of the membrane by pulsed field gradient spin echo NMR (PGSE-NMR).	100-500**	➢ Promising for polymeric thin film characterization	Saito et al. (2004) Hansen et al. (1996)
	Small-angle neutron scattering (SANS)	Measurement of neutron scattering of water molecules retained in the membrane pores	>1.9	➢ Non-destructive technique	Stefanopoulos et al. (1999)
	Electron spin resonan-ce (ESR)	The technique works on the same principle as NMR spin relaxation, but now spin transitions of unpaired electrons are recorded.	-	-	Khulbe and Matsuura (2000)
	Electrokinetic phenomena	Modification of the induced streaming and membrane zeta potential	-	➢ Only simulation studies have been reported.	Saksena and Zidney (1995)

* SEM: Scanning Electron Microscopy; TEM: Transmission Electron Microscopy; FESEM: Field Energy Scanning Electron Microscopy; AFM: Atomic Force Microscopy.

** Only the PSD range indicated is reported.

Furthermore, most of these methods (e.g., gas adsorption-desorption, gas/liquid and liquid/liquid porometry, mercury porosimetry, microscopy techniques,…) are unsatisfactory for the determination of PSDs in asymmetric membranes, because they are unable to discriminate between the active separation layer and the bulk porous support (*Jakobs and Koros, 1997*), since it only constitutes a very small fraction of its material. Due to the large difference in pore size and pore volume of the active layer and the support, the characterization of the selective layer typically lacks detail and resolution and the results are difficult to interpret in many cases.

An alternative approach could focus on relating permeation measurements in porous membranes with the nature of their PSDs. The characterization of PSDs via direct liquid, gas or solute permeation measurements might have the great advantage of enabling the determination of PSDs under conditions similar to those in which the membrane is likely to be used. In fact, the permeation mechanisms of a membrane provide a set of suitable moment generating functions from which, by means of ***moment theory***, its PSD can be derived without any previous assumption about its nature.

Although some earlier works had experimentally assessed the relationship between the solute sieving ability of porous membranes and the size of different monodisperse solutes in an attempt to obtain information about PSDs (*Leypoldt, 1987; Aimar et al., 1990; Singh et al., 1998; Lee et al., 2002*), the first applications of moment theory to the membrane field were reported by *Knierim et al. (1984)* and by *Knierim and Mason (1989)*, who proposed the determination of upper and lower bounds on the cumulative PSD of porous membranes by using, respectively, diffusion-convection and solute sieving moment generating functions. The information about a PSD is captured because the diffusion-convection and the sieving behavior of monodisperse solutes also vary with the pore size. The former function takes advantage of the fact that diffusion and convection depend differently on pore size and therefore the relative contribution of each to the overall solute transfer rate (by changing the solute Pe number, N_{Pe}) varies with the pore size, while the latter is based on the dependence of the reflection coefficient for large monodisperse solutes on the pore size at large N_{Pe}.

More recently, *Baltus (1997a, 1997b)* carried out theoretical calculations with model membranes containing log-normal distributions that revealed that narrow bounds can be placed on the cumulative PSD of a UF model membrane by the measurement of its pure liquid permeability together with (1) one or two sieving measurements at $N_{Pe}>>1$, (2) one or two diffusion-convection fluxes of a small, non-hindered solute at $N_{Pe}\sim1$, or (3) one or two large solute hindered diffusivity measurements. All these three set of moment generating functions were reported to allow the discrimination between membranes with the same mean pore size, but with different PSDs. It should be stressed that diffusion, either directly or indirectly,

reveals to be the key process in the generation of the consistent set of moment generating functions above indicated.

In a subsequent step, in light of these comments, *Pera-Titus et al. (2006d)* showed how permeation measurements in porous UF and NF asymmetric membranes might be directly related to a PSD through the use of moment theory and provided experimental evidence of the feasibility of the method developed for the determination of log-normal PSDs of UF, NF and MF asymmetric commercial membranes. Relevant data concerning the PSD of membrane could be obtained by performing three independent experiments: (1) pure liquid permeability, (2) pure gas Knudsen diffusion permeance, and (3) non-hindered diffusion of an electrolyte (e.g., HCl). The main advantage of this procedure relies not only on its conceptual simplicity, but also on the easiness of its practical implementation as a first insight into the pore structure of a porous membrane.

I.2.4. Pervaporation

I.2.4.1. General concepts

Pervaporation (PV) is a membrane-based separation process that has gained increasing interest by the chemical industry as an effective and energy-efficient technology to carry out separations that are troublesome or difficult to achieve by conventional means (i.e. distillation, extraction or adsorption), such as azeotropic and close-boiling liquid mixture separation, organic solvent dehydration and recovery of high added-value dilute species from water (*Feng and Huang, 1997; Lipniki et al., 1999*). The technique is termed "pervaporation" because it involves the permselective "vaporization" of a liquid mixture (feed) through a suitable membrane whose downstream pressure is usually kept under vacuum (***Vacuum Pervaporation, VPV***) or that can be swept by a gas (***Sweep Gas Pervaporation, SGPV***) in the special case that the permeate can be discharged without condensation. Besides these two modes of operation, there are several other process variants, including thermal pervaporation, osmotic distillation, saturated vapor permeation, and pressure-driven pervaporation (*Feng and Huang, 1997*). Because different species permeate through the membrane at very different rates, a substance at low concentration in the liquid feed can be highly enriched in the vapor permeate. Thus, separation occurs, being the pervaporative efficiency strongly determined by the physicochemical nature of the membrane and by the kind of feed mixture to be separated.

I.2.4.2. Pervaporation with polymeric membranes

Since the earlier works of Heisler and Binning in the late 50s (*Huang, 1991*), polymeric membranes have been widely investigated for PV membrane-based solvent separations and for

reactive separations (either alone or integrated into hybrid distillation or extraction processes) (*Feng and Huang, 1997; Fleming, 1992; Jonquieres et al., 2002; Keurentjes et al., 1994; Lipniki et al., 1999*). However, their practical use has been limited due to the insufficiency of their thermal, mechanical, and chemical stability (*Feng and Huang, 1997*). To overcome these shortcomings and to improve the membrane multipurpose character, extensive research has been directed in the last decades towards the development of inorganic membranes with suitable PV performance (*Coronas and Santamaria, 1999*).

Subsequently, substantial work was done to extend pervaporation for the separation of many liquid mixtures and to a variety of membranes. The applications of pervaporation concern (i) dehydration of organic sorbents, (ii) removal of organic compounds from aqueous solutions (recover of valuable organic species and for groundwater purification and wastewater treatment), and (iii) separation of anhydrous organic mixtures. Polymeric membranes have been widely tested for the separation of liquid mixtures including, for example, alcohols/water, acetone/water, methanol/MTBE, methanol/pentane, toluene/heptane and isomeric xylenes. Nowadays, there are over 100 pervaporation plants throughout the world, most of them to dehydrate organic solvents as ethanol and propanol (*Wynn, 2001*). However, this technology has not yet become widely extended, because of the high equipment costs, the difficulties in fabricating the unit, and the low stability of the polymeric membranes.

I.2.4.3. Pervaporation vs. distillation

Pervaporation has attracted widespread attention by industry as an energy efficient technique for the separation of azeotropic or close-boiling liquid mixtures, and for the dehydration of organic solvents in many chemical and pharmaceutical processes (*Feng and Huang, 1997; Shah et al., 1999*). Pervaporation offers the following general advantages in front of the conventional distillation:

- It reduces the demand of energy, because only the liquid fraction to be separated is vaporized.
- The equipment is simple, because only a vacuum pump or a stream of sweep gas is needed
- High selectivity
- Low operating costs
- Lower thermal degradation of materials sensible to heat
- It is not limited by azeotropes
- It does not produce emissions to the environment

In many practical applications (see Table I.5), pervaporation is only competitive to distillation for separation of azeotropic or close-boiling liquid mixtures. When the volatility of the major species is higher than that of the minor, pervaporation allows to save the energy required to vaporize the former. Distillation is a more extended separation method in mixtures where the organic species is less volatile than water, because the energy requirements are lower (*Wynn, 2006*).

Table I.5: Applications of pervaporation (*Feng and Huang, 1997*)

APPLICATIONS	*DETAILS*
Separation of water from organic/water mixtures	Separation and/or dehydration of water/organic azeotropes (H_2O/EtOH, H_2O/IPA, H_2O/pyridine)
	Dehydration of organic solvents
	Change in the equilibrium of reaction (e.g., esterification)
Extraction of volatile species from aqueous and gaseous streams	Extraction of chlorinated hydrocarbons
	Separation of aromatic species
	Dealcoholization of beer and wine
	Extraction of volatile organic species from air
Separation of organic/ organic mixtures	Separation of azeotropes (e.g., EtOH/cyclohexane, MeOH/MTBE, EtOH/ETBE)
	Separation of isomers (e.g., xylenes)

I.3. ZEOLITES

The term *zeolite* (from the Greek words *zeo*: to boil and lithos: *stone*) designates a variety of crystalline, hydrated and microporous aluminosilicates of general formula $M_{x/n}\cdot[(AlO_2)_x\ (SiO_2)_y]\cdot zH_2O$ with a framework structure based on a well-defined system of channels and cavities. This term was first proposed by the Swedish geologist A.F. Cronstedt in 1756 for a family of natural minerals whose main properties are the exchange of ions and a reversible desorption of water. Since then, more than 135 types of zeolites have been reported, either natural or artificial (*Ramsay and Kallus, 2000; Atlas of zeolites, 2002*). According to the symmetry of their structure, zeolites are usually classified with a three-letter code given by the International Zeolite Association (IZA) (http://www.izastructure.org).

I.3.1. Framework structure

The basic elements of the zeolite frameworks are TO_4 tetrahedra (T = Si, Al) linked each other through the oxygen atoms. According to the IUPAC, the description and

classification of the topology of zeolites is based on the concept of larger units known as ***secondary building units*** (SBUs) proposed by Meier in 1967. These can consist, for instance, of simple rings and prisms of various sizes. By combining such basic units, the known zeolite frameworks can be constructed. For instance, LTA consists of single-4-ring, single-6-ring and double-4-ring (D4R), while FAU consists of single-4-ring, single-6-ring and double-6-ring (D6R). Alternative concepts are based on more complex chains or layer structures known as ***structural subunits*** (SSUs).

The various zeolite structures differ not only in the type and dimensionality of their pore systems, but also in the size of their pore apertures. According to this latter aspect, zeolites can be broadly classified as: narrow-pore (0.35-0.45 nm), medium-pore (0.45-0.60 nm), wide-pore (0.60-0.90 nm) and super-wide pore (>0.90 nm). Sodalite (SD) and zeolite A (LTA) can be catalogued as narrow-pore zeolites, zeolite ZSM-5 (MFI) as medium-pore, and zeolites X, Y (FAU) and mordenite (MOR) as wide-pore. The regular nature of the pores and their apertures, whose dimensions are of the same order of magnitude as the kinetic diameters of molecules (see Figure I.2a), enables zeolites to behave as molecular sieves. This is an outstanding property that gives zeolites their value as selective adsorbents for separating substances and as shape-selective catalysts. Depending on the type of zeolite and its pore system (see Table I.6), the molecules can penetrate into the cavity system or can be excluded from it. Zeolitic pore structures can be classified in two groups as illustrated in Figure I.2b. While LTA and FAU type zeolites have super-cages in their structures, MFI and MOR type have cylindrical structured pores.

In addition, the cations required to compensate the negative structural charge due to the presence of AlO_4 occupy well-defined positions in the cavities or channels. Their nature and distribution throughout the zeolitic structure is relevant in terms of their applications, because the effective pore diameter of zeolites depends on the kind and number of cations present.

I.3.2. Physical and chemical properties of zeolites

Most of chemical and physical properties of zeolites are essentially determined by their framework aluminum content, which is usually expressed by the Si/Al or SiO_2/Al_2O_3 ratio. According to the *Loewenstein rule* (*Barrer, 1982*), Al-O-Al groups cannot occur in crystalline aluminosilicates, and therefore a SiO_2/Al_2O_3 ratio <2 is far impossible for zeolites. Each zeolite structure type exhibits a phase breadth with respect to the SiO_2/Al_2O_3 ratio. A distinction can be made between low-silica (SiO_2/Al_2O_3<4), intermediate-silica (4<SiO_2/Al_2O_3<20), and high-silica (20<SiO_2/Al_2O_3<200) zeolites. An increase in the silica content leads to an increasingly hydrophobic character, occurring the transition from hydrophilic to hydrophobic behavior at a SiO_2/Al_2O_3 ratio ca. 20. The most hydrophilic zeolite

is zeolite A (LTA) having a ratio SiO_2/Al_2O_3 = 2, while the most hydrophobic is silicalite-1 (MFI), having no aluminum in its structure. The SiO_2/Al_2O_3 ratio can be varied in some range, keeping the structure almost the same. For example, the zeolite with FAU structure having SiO_2/Al_2O_3 ratio around 2-3 is called zeolite X, while that with a ratio 3-6 is called zeolite Y.

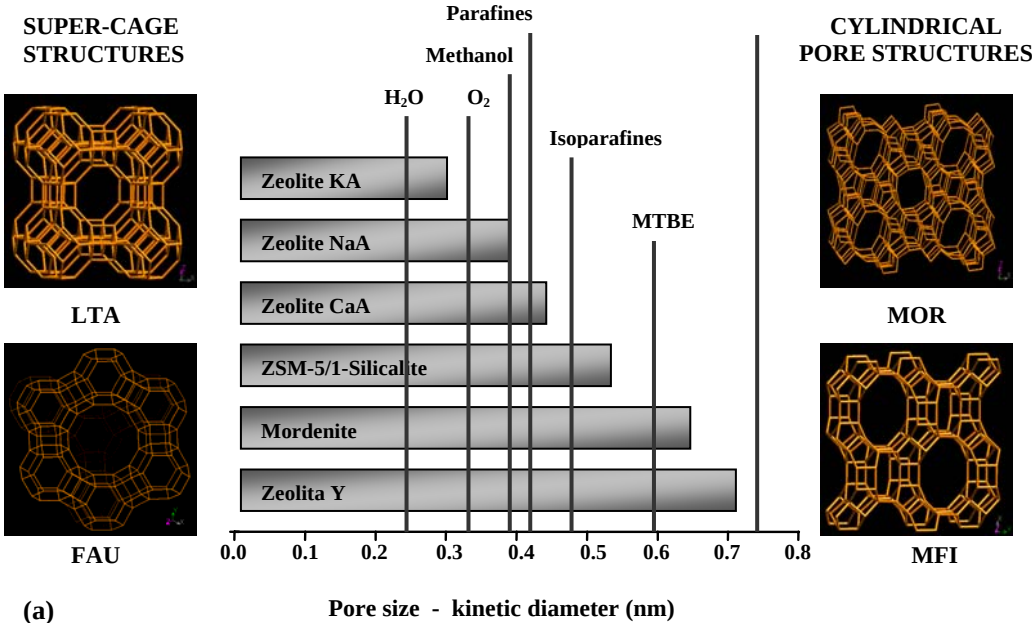

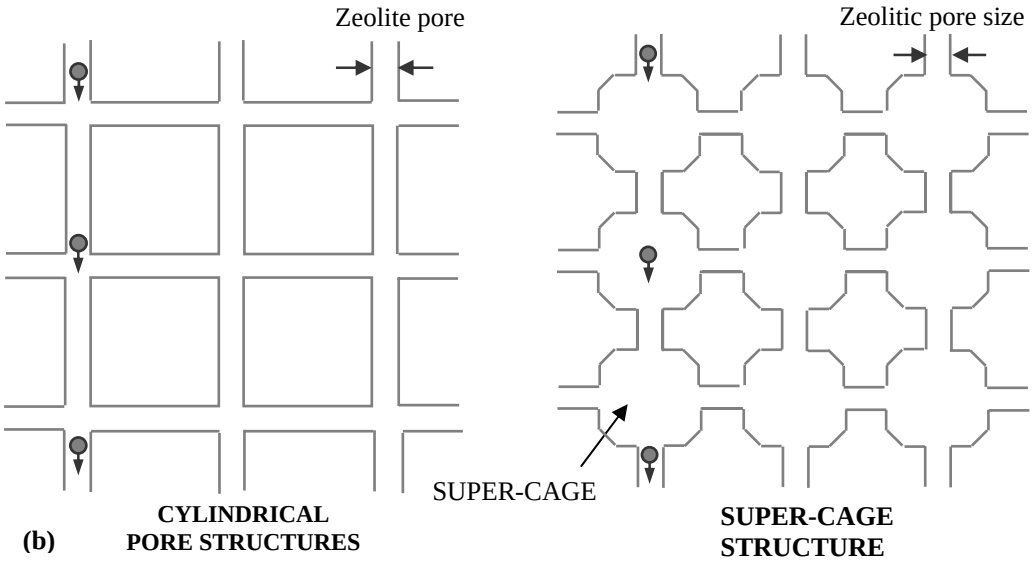

Figure I.2: (a) Mean pore size of some zeolites and kinetic diameter of several molecules; (b) Zeolitic pore structures

Table I.6: Summary of the structural features of the main zeolites (*Bond, 1987; Ullmann's, 1998*)

Zeolite [1]	*Structure Type*[2]	*No. tetrahedra in the ring*	*Pore apertures [nm]*	*FD*[3]	N_T[4]	SiO_2/Al_2O_3 *molar ratio*
Zeolite A	LTA	8	0.41	12.9	24	2.0-6.8
Zeolite P	GIS	8	0.31 x 0.45 0.28 x 0.48	12.9	24	2.0-5.0
ZSM-5 / Silicalite-1	MFI	10	0.53 x 0.55 0.51 x 0.56	17.9	96	25- ∞
Zeolite X Zeolite Y	FAU	12	0.74	12.7	192	2.0-3.0 3.0-6.0
Mordenite	MOR	12	0.65 x 0.70 0.26 x 0.57	17.2	48	9.0-35

[1] The dimensionality of zeolites A, P, X and Y is 3 and 2 for mordenite and ZSM-5. The density of these zeolites is in the range 1.9-2.3 g cm^{-3}.

[2] Code used by the International Zeolite Association (IZA)

[3] Density of the structure in number of tetrahedral atom per $Å^3$

[4] Number of tetrahedral positions in a unit cell

The surface selectivity of zeolites as adsorbents also depends on the SiO_2/Al_2O_3 ratio. Aluminum-rich zeolites preferentially adsorb strongly polar molecules, and are therefore widely used as drying agents. Furthermore, due to the mobility of cations in their cavities and channels, zeolites exhibit ionic conductivity, which depends on the diameter of the channels, the nature and concentration of the cations in the structure, and the water content. This property is of high importance, because it makes them suitable for applications as ion-exchangers (up to 650 meq/100 mg).

On heating, hydrated zeolites release water. Many zeolites can be almost completely free of adsorbed water without major alteration of their crystal structure after calcination at 700-800 K, leaving solids with large free micropore volumes (even greater than 50% of the volume) and inner surfaces whose extent depends on the framework density of the particular zeolite framework and on the number and nature of cations. Moreover, in spite of their open structure, zeolites have remarkably good thermal stability, which also varies with the zeolite framework, but more with the SiO_2/Al_2O_3 ratio and the nature of cations. As a general rule, zeolites are thermally stable up to 1000 K and they also show a high hydrothermal stability, namely the ability to retain their structure without undergoing any phase transformation in the presence of water vapor.

Strong acids decompose low-silica zeolites such as NaA and NaX by dissolving the aluminum atoms out of the framework, with the consequent breakdown of the crystal

structure. By increasing the SiO_2/Al_2O_3 ratio, zeolites become less sensitive to dealumination by acids, being high-silica zeolites structurally stable even in a strong mineral acidic environment. On the other hand, aqueous alkalis lead to phase transitions in high-aluminum zeolites and to dissolution in very high-silica zeolites.

I.3.3. Zeolite A

According to the IUPAC, zeolite A belongs to the LTA group (Linde Type A). The fully hydrated Na-exchanged LTA structure, of general formula $Na_{12}(Si_{12}Al_{12}O_{48})\cdot 27H_2O$, is built up by truncated cubo-octahedron units known as sodalite or β-cages (diameter 0.66 nm), which are linked together via the cubic D4R units to form larger cavities α-cages (diameter 1.23 nm) with the shape of a truncated cubo-octahedron (see Figure I.3) that are interconnected by windows formed by rings consisting of 8 atoms (either Si or Al) of 0.41 x 0.41 nm, generating a uniform 3D pore system according to the cubic system (a=b=c=2.46 nm; α=β=γ=90º) at which zeolite NaA crystallizes. It should be noted that, when fully hydrated, the α- and β-cages have space for 20 and 4 water molecules, respectively, while the 8-rings contain 3 molecules of water.

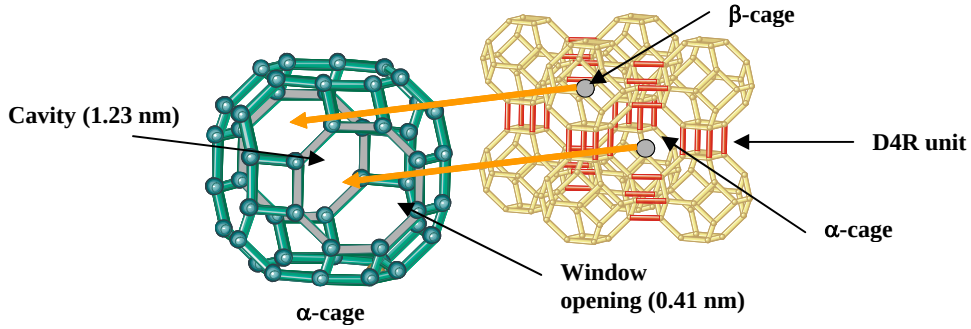

Figure I.3: Unit cell of the structure LTA

The general physical and chemical properties of zeolite NaA are summarized in Table I.7. Because zeolite A is a low-silica content zeolite, its framework is rich in sodium ions. Therefore, zeolite A presents a high ionic conductivity and a high ion-exchange capacity, but it is not stable in acid and alkaline environments, because it can suffer from dealumination. Furthermore, zeolite A shows a hydrophilic character, namely, it tends to adsorb polar molecules, in particular water. The aluminum positions show an acid nature (see Figure I.4). Zeolite A is directly used as additive in detergents and constitutes the essential material of a great variety of adsorbents which are used in many separation and purification processes. The

position of sodium ions in the cages is important, because they act as adsorption sites. Among the total number of sodium atoms in a unit cell, 12, 8 of them are placed inside the α-cage, while the other 4 are placed in the β-cages. Therefore, α-cages play a more important role than β-cages in the adsorption process of small molecules.

Table I.7: Physical and chemical properties of zeolite NaA

FORMULA		$Na_{12}[(AlO_2)_{12}\cdot(SiO_2)_{12}]\cdot 27H_2O$
COLOR		White
DENSITY		~2.00 g cm^{-3}
STABILITY	Thermal	< 933 K
	Chemical	To acid ⇒ It dissolves at a pH <6 To alkali ⇒ Phase transition to hydroxysodalite
SOLUBILITY		Negligible
pH IN AQUEOUS SOLUTION		9 – 12 (partial hydrolysis)
SiO_2/Al_2O_3 RATIO		2.0 – 6.8
ION-EXCHANGE		> 160 mg CaO/g dry zeolite NaA (20°C)

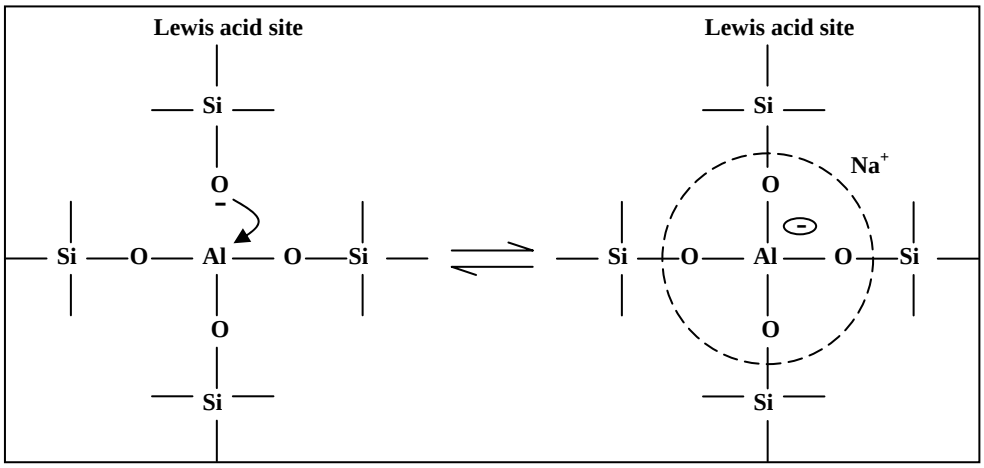

Figure I.4: Representation of the acid sites of zeolite NaA (*Bond, 1987*)

I.3.4. Preparation of zeolites

Zeolites are usually formed as powder of micrometer size by spontaneous nucleation and growth in a synthesis gel (hydrogel) or solution under hydrothermal conditions, although

crystals up to 5 mm can be produced under special conditions. The synthesis gel/solution usually contains the silicate and aluminate precursors, an alkaline component (generally sodium), water and might also include a structure directing agent (SDA), which is sometimes referred in the literature as template. The use of a SDA is necessary to synthesize zeolites with high SiO_2/Al_2O_3 ratios, which must be subjected to a calcination step after their preparation to remove water and the SDA filling the zeolite pores.

Figure I.5 shows schematically the general mechanism of zeolite synthesis. The synthesis gel is constituted by a number of long-chain polymers and cycles formed from the polymerization of the aluminate and silicate precursors. The composition and structure of the hydrated gel are strongly dependent on the shape and structure of the polymerizing species, in such a way that a change in the chemical composition and molecular weight of the initial species in the precursor solutions might leads to a change in the gel structure, which might in its turn involve a change in the zeolite phases that are finally obtained. In the process of crystallization of the gel under hydrothermal conditions, the alkaline ions and the aluminate and silicate chains react and tend to build free TO_4 units due to the depolymerization of the gel caused by the presence of HO^- ions and by the effect of temperature. Subsequently, TO_4 units are reordered to build SBUs that polymerize to form polyhedral nuclei that grow to form larger zeolite crystals. The nature of the final zeolite/s obtained is strongly determined by the synthesis conditions, namely by the kind of precursors used as reactants, their concentration, the pH, the synthesis time and the temperature.

One of the main characteristics of the synthesis of zeolites is the existence of an induction period, namely the presence of a time (usually several hours) at the beginning of the synthesis with no detectable crystal formation. In this period, zeolite nuclei are spontaneously formed that allow further crystal growth. The rate of nucleation and growth of crystals is often described by a population balance model (*Barrer, 1982*). The crystal size shows a linear increase with the synthesis time, while the crystallinity of zeolites shows a S-shaped curve. Higher pH or temperature, or aging results in shorter crystallization time.

Nucleation and growth mechanisms constitute one of the major topics in zeolite science. Two mechanisms have been suggested by *Barrer (1982)*: (1) direct transformation of the synthesis gel into the zeolitic crystalline structure, and (2) dissolution of the gel to form a clear solution and crystallization via soluble species. Seed crystals or initial-bred nuclei are sometimes used to study the growth mechanisms (*Gonthier and Thompson, 1994; Gora et al., 1997*), which grow under the synthesis conditions to form the same zeolite type as the seed crystal and promote the rate of formation of zeolite crystals (*Warzywoda et al., 1991*).

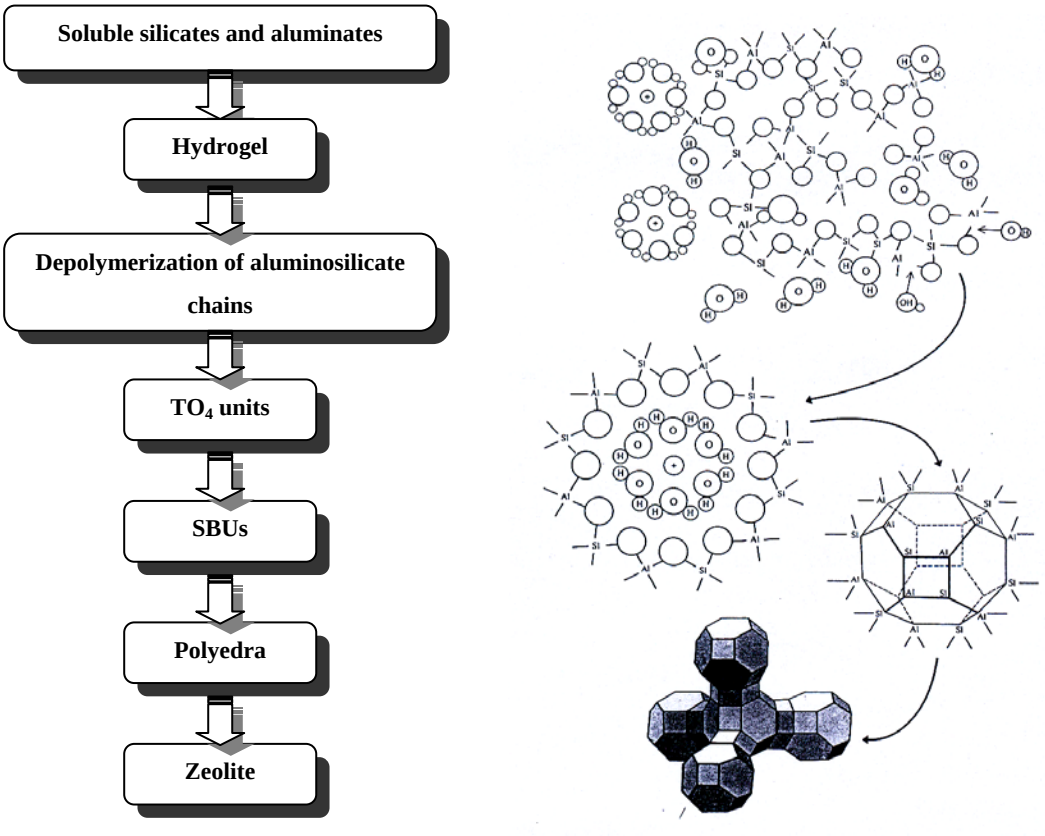

Figure I.5: Scheme of the steps involved in the zeolitization process (Breck, 1984)

I.3.5. Applications of zeolites

The most relevant applications of zeolites are related to their adsorptive and ion-exchange properties. In this way, zeolites are generally employed as:

- **Detergent additives**: Zeolite NaA constitutes the most extended zeolite in use due to its high ion-exchange behavior, which enables it to capture and remove harmful ions from water responsible for its hardness (Ca^{2+}, Mg^{2+}) and also trace ions of heavy metals (e.g. Cu^{2+}). This zeolite has allowed the substitution of phosphate additives in detergents for hardness reduction, because they are unsuitable due to environmental reasons.

- **Adsorbents**: Zeolites are relevant industrial adsorbents with a widespread field of applications not only in the adsorption of species, but also in separation and purification processes due to their high selectivities. Zeolites A and X are the most

employed zeolites in adsorption processes, both in gaseous and liquid phases. Their main applications in this field are the following ones:

- Adsorption of water from gaseous and liquid streams with zeolites A and Y
- Air and gas purification: removal of CO_2, H_2S, dioxins, elemental Hg,… with zeolites A, X, Y and silicalite-1)
- Separation of mixtures: O_2/N_2, n-alkanes/i-alkanes, xylene isomers,… with zeolites A and X

➢ **Catalysts**: Except for zeolites A and X, which are not stable in acidic conditions, zeolites can be transformed into the acidic form, exhibiting Brϕnsted or Lewis acidity, which confers them catalytic activity. Furthermore, zeolites show shape selectivity when their pore sizes are similar to the kinetic diameters of the molecules. Three different kinds of shape selectivity can be proposed: to reactants, to products, and to transition states, if the limiting step is, respectively, the penetration of a reactive, the formation of a product, or the formation of an intermediate species inside the zeolitic structure. Zeolite catalysts are mainly used in the following four industrial fields:

- Oil refining: Fluid catalytic cracking (FCC), for which zeolites Y and ZSM-5 are used.
- Gas conversion: Transformation of methanol (synthesis gas) into mineral oils and petrochemical products with zeolite ZSM-5.
- Petrochemistry: Production of etylbenzene and isomerization of xylene with zeolites ZSM-5, mordenite,…
- Environmental protection: Reduction of NO_x.

I.3.6. Adsorption equilibrium on zeolites

I.3.6.1. Unary adsorption equilibrium of gases and vapors on zeolites

The adsorption equilibrium of a single gas or vapor (***unary adsorption equilibrium***) is one of the most outstanding properties of zeolites. Molecules adsorb on zeolites because of the intermolecular attractive forces between the adsorbent (zeolite) and the adsorbate (gases and vapors). The entire void volume of zeolites represents a space where an adsorption field exists. On the grounds of the regularity in their internal microporous system, zeolites usually show

Type I adsorption isotherms according to the Emmett-Teller classification or the Langmuir-type isotherm. In the most general situation, the generalized Langmuir isotherm (LG) is usually used to account the adsorption equilibrium process in an energetically heterogeneous surface, where the molar loading, **q(P)** [mol kg^{-1} of adsorbent] can be obtained by solving the General Integral Equation for Adsorption through the use of the Langmuir equation for local molar loading, $\mathbf{q_L}$ [mol kg^{-1}] (Eq. I.4)

$$q(P) = \int_{E_{min}}^{E_{max}} q_L(P,E)\chi(E)\delta E \qquad \text{(Eq. I.4)}$$

where **P** is the pressure [kPa], **χ(E)** is the distribution function of adsorption energies, which takes values from the minimum energy, $\mathbf{E_{min}}$, to the maximum one, $\mathbf{E_{max}}$. The generalized Langmuir equation can be deduced by Eqs. I.5 and I.6:

$$\theta = \frac{q}{q_M} = \left(\frac{y}{1+y}\right)^{\beta}, \qquad \text{(Eq. I.5)}$$

$$\text{with} \quad y = (K\,P)^{\delta} = (K_{\infty}\,P)^{\delta}\exp\left(-\delta\frac{\Delta H^{o}}{RT}\right), \qquad \text{(Eq. I.6)}$$

where $\mathbf{q_M}$ is the molar saturation loading [mol kg^{-1}], **K** is the adsorption equilibrium constant [kPa^{-1}], $\mathbf{K_\infty}$ is a preexponential factor that contains the entropy of adsorption [kPa^{-1}], $\mathbf{\Delta H^o}$ is the adsorption enthalpy [kJ mol^{-1}], and $\theta = q/q_M$ is the fractional occupancy [-]. The resolution of the generalized Langmuir Isotherm allows to obtain a number of adsorption isotherms depending on the relative valued of parameters β and δ. As shown in Table I.8, the generalized Langmuir Isotherm tends to the single-site Langmuir (L) isotherm for $\beta = \delta = 1$, the generalized Freundlich (GF) isotherm for $0 \le \beta \le 1$ and $\delta = 1$, the Langmuir-Freundlich (LF) isotherm for $\beta = 1$ and $\delta < 1$, and the Tóth (T) isotherm for $\beta > 1$ and $0 < \delta \le 1$.

Table I.8: Isotherms derived from the generalized Langmuir Isotherm

Adsorption isotherm	*β [-]*	*δ [-]*	*Equation*	*Eq. number*
Single-site Langmuir	1	1	$q_i = q_{M,i}\frac{K_i P_i}{1+K_i P}$	Eq. I.7
Generalized Freundlich [1]	$0 \le \beta \le 1$	$\delta = 1$	$q_i = q_{M,i}(K_i P_i)^{\beta\delta} = K_{f,i} P_i^{1/n}$	Eq. I.8
Langmuir-Freundlich	$\beta = 1$	$0 \le \delta \le 1$		
Tóth [2]	$\beta > 1$	$0 \le \delta \le 1$	$q_i = q_{M,i}\frac{K_i P}{\left[1+(K_i P_i)^{\delta}\right]^{1/\delta}}$	Eq. I.9

[1] $1/n = \beta\,\delta \le 1$

[2] For simplicity, $\beta = 1/\delta > 1$ is chosen

The adsorption of water and alcohols on zeolite A and mordenite usually follows the single-site Langmuir isotherm (*Yamazaki and Tsutsumi, 1997; Okamoto et al., 2001*). It should be noted that the molar saturation loading, which is the maximum number of molecules adsorbed in the pore volume, is not expected to depend on temperature if the zeolite structure, and thus the total pore volume, does not change with temperature. Instead, saturation loadings are only expected to depend on molecular size. Furthermore, according to the Gurvitsch's rule (*Breck, 1984*), usually fulfilled by zeolites, the saturation loading is proportional to the liquid density of the adsorbate.

On the other hand, larger molecules and molecules at high loadings might show preference for specific adsorption sites in the zeolite pores. For this special situation, adsorption is usually better represented by a dual-site Langmuir adsorption isotherm (Eq. I.10)

$$q = q_{M,A}\frac{K_A P}{1+K_A P} + q_{M,B}\frac{K_B P}{1+K_B P} \quad [\text{mol kg}^{-1}], \qquad \text{(Eq. I.10)}$$

where the subscripts **A** and **B** indicate independent adsorption sites, which are usually the channels and intersections within a zeolite framework. The adsorption of hexane and butane isomers on silicalite-1 usually follows a dual-site Langmuir adsorption isotherm because the linear molecules preferentially adsorb in the channels of silicalite, while the branched prefer the intersections (*Krishna et al., 2001; Zhu et al., 2001; Gardner et al., 2004*).

Modified versions of the Langmuir isotherm such as the Tóth and Unilan isotherms have also been proposed to account for the adsorption equilibrium in zeolites. *Zhu et al. (2005)* used the Unilan isotherm to fit experimental adsorption data of water, CO, H_2 and CH_4 on zeolite A. In addition, *Sakuth et al. (1998)* proposed the Tóth isotherm to fit adsorption data of toluene and 1-propanol vapors on zeolite Y. It should be noted that the Freundlich and Temkin isotherms show limited applicability to zeolite adsorption. Furthermore, *Ruthven (1984)* derived an isotherm for cage-type structures using statistical mechanics. For a maximum of two molecules per cage, the relation between the amount adsorbed and the pressure is given by Eq. I.11

$$\theta = \frac{K P + (K P)^2 (1 - 2\beta/V)^2}{1 + K P + \frac{1}{2}(K P)^2 (1 - 2\beta/V)^2} \qquad \text{(Eq. I.11)}$$

where β and **V** are, respectively, the effective molecular volume [m^3] and the volume of the cage [m^3]. Although the Langmuir-type (single- and dual-site) isotherm has been extensively applied with some degree of success for the description of the unary adsorption equilibrium on zeolites, the break in the isotherm actually corresponds to the filling of the microvoids and not

to the completion of a monolayer. Moreover, the Langmuir isotherm assumes that the adsorption potential is uniform alongside the zeolite structure, namely, no energetic heterogeneity exists, which is not true in most cases of zeolite adsorption. In order to overcome these shortcomings, some empirical theories like the Polyani potential theory were developed in the past for treating adsorption, which was further modified by Dubinin and Astakhov to account for the adsorption process in microporous materials (*Breck, 1984*). In the Polyani theory, the characteristic isotherm relates the molar loading, **q**, at temperature **T** and equilibrium partial pressure **P** with its work of adsorption, **A** [kJ mol^{-1}] by Eq. I.12

$$q(P) = q_M \exp\left[-\left(\frac{A}{E^o}\right)^{\alpha}\right] \quad [\text{mol kg}^{-1}], \qquad \text{(Eq. I.12)}$$

where $\mathbf{E^o}$ is a characteristic energy [kJ mol^{-1}] that accounts for the interaction between the adsorbate and the adsorbent, and α [-] is a property of the zeolite material and adsorbate. For the special case α**=2**, the isotherm is usually referred to as "Dubinin-Raduskevich." The work of adsorption, **A**, can be related to the reduced pressure, $\Pi = P/P^o$ [-], by Eq. 1.13

$$A = -RTLn\left(\frac{P}{P^o}\right) = -RTLn(\Pi) \quad [\text{J mol}^{-1}] \qquad \text{(Eq. I.13)}$$

Combining Eqs. I.12 and I.13 and taking logarithms, Eq. I.13 is finally used to describe the adsorption equilibrium process in zeolites:

$$Ln(\theta) = Ln\left(\frac{q}{q_M}\right) = -\left[-\frac{RT}{E^o}Ln(\Pi)\right]^{\alpha} \text{ [-]} \qquad \text{(Eq. I.14)}$$

On the other hand, the thermodynamic analysis of the adsorption equilibrium of gases in microporous materials has been usually visualized as a process that occurs at the surface of the solid adsorbent (*Ruthven, 1984; Yang, 1987; Valenzuela and Myers, 1989; Suzuki, 1990*). Key concepts in the thermodynamics of surface adsorption (2D) such as interfacial area, A, and ***spreading*** *or* ***interfacial pressure,*** π [N m^{-1}], which corresponds to the effective pressure at which a molecule adsorbs, have no sense when dealing with microporous materials (*Myers, 2002*). In fact, instead of adsorbing on its surface, gas molecules adsorb in the microporous volume of the adsorbent. Otherwise, the concept of ***surface potential***, Φ [J kg^{-1}], in the field of solution thermodynamics (3D), is usually preferred for microporous materials (*Myers, 2002; Llorens, 2005*), which corresponds to the potential at which a molecule adsorbs. The spreading pressure and the surface potential themselves cannot be measured, but can be derived using a modified Gibbs-Duhem equation under isothermal conditions (*Yang, 1987*) as described below.

In general terms, solution thermodynamics assumes that the adsorption system consists of three phases: gas or vapor phase (g), solid phase (s) and adsorbed phase (a). The adsorbed phase has no volume, $\mathbf{V_a = 0}$, and, together with the solid phase, it constitutes the condensed phase (v). The volumes of all phases are assumed not to change along the adsorption process. The volume of the gas phase, $\mathbf{V_g}$, is fixed considering that helium, as a reference gas, does not adsorb at near-ambient temperature and atmospheric pressure. The volume of the gas phase includes the volume related to micropores. For this situation, the differential equation for the internal energy of the condensed phase implies that

$$\delta U = T\,\delta S - P\,\delta V + \mu\,\delta n + \mu'\delta m_S \qquad \text{(Eq. I.15)}$$

where the independent variables of the internal energy are: temperature, **T** [K], pressure, **P** [kPa], chemical potential of the adsorbate, **μ** [J mol^{-1}], and chemical potential of the adsorbent, **μ'** [J kg of $adsorbent^{-1}$]. The internal energy is an homogeneous function of 1st order of the extensive variables: entropy, **S** [J K^{-1}], volume, **V** [m^3], amount of adsorbate, **n** [mol], and weight of solid adsorbent, $\mathbf{m_S}$ [kg], all in the condensed phase. The application of the Euler theorem to the function *U = U(S, V, n, m)* allows to obtain Eq. I.16

$$U = T\,S - P\,V + \mu\,n + \mu'\,m_S \qquad \text{(Eq. I.16)}$$

A more convenient way to express Eq. I.16 is per unit mass of adsorbent through the use of specific extensive variables (with the symbol – on top). Therefore, Eq. I.17 can be obtained:

$$\overline{U} = T\,\overline{S} - P\,\overline{V} + \mu\,q + \mu', \qquad \text{(Eq. I.17)}$$

where $\mathbf{q = n / m_S}$ is the molar loading [mol kg^{-1}]. For the pure solid adsorbent phase, Eq. I.17 transforms into Eq. I.18:

$$\overline{U}^S = T\,\overline{S}^S - P\,\overline{V}^S + \mu'^S \qquad \text{(Eq. I.18)}$$

where $\mathbf{\mu'^S}$ [J kg^{-1}] is the chemical potential of the pure adsorbent without adsorbate. On the other hand, the internal energy and entropy per kg of adsorbent of the condensed phase include, respectively, the contributions of the internal energies and entropies related to the adsorbed and solid phases. The relevant specific extensive thermodynamic variables for the adsorbed phase are defined by Eqs. I.19

$$\overline{U}^a = \overline{U} - \overline{U}^S \qquad \text{(Eqs. I.19)}$$
$$\overline{S}^a = \overline{S} - \overline{S}^S$$
$$\overline{V}^a = \overline{V} - \overline{V}^S$$

The application of the 1st Principle of Thermodynamics to the adsorbed phase ($V_a = 0$) allows to write the differential equation for the intensive internal energy of the adsorbed phase in terms of specific extensive variables (Eq. I.20)

$$\delta\overline{U}^{a} = T\,\delta\overline{S}^{a} + \mu\,\delta q \qquad \text{(Eq. I.20)}$$

In its turn, Eq. I.19 allows to write Eq. I.21 that accounts for the specific Gibbs free energy (or simply free energy or enthalpy) of the adsorbed phase

$$\overline{G}^{a} = \overline{U}^{a} - T\,\overline{S}^{a} + P\,\overline{V}_{a} = \mu\,q + \Phi \qquad \text{(Eq. I.21)}$$

where Φ is the surface potential [J kg of adsorbent^{-1}] that equals $\mu' - \mu'^{S}$. The specific free energy of the adsorbed phase includes two contributions: (1) free energy of **q** moles adsorbed per kg of adsorbent at equilibrium with the gas phase namely, with the same chemical potential, and (2) the surface potential, **Φ**, which depends on the interaction between the adsorbate molecules and the adsorbent and tends to zero when there is no adsorption. the interaction between the adsorbate and adsorbent molecules alters the surface potential of *the adsorbent*, and therefore the free energy of the adsorbed phase. The differentiation of Eq. I.21 and further combination with Eq. I.20 allows to obtain Eq. I.22

$$d\overline{G}^{a} = \overline{S}^{a}\,\delta T + \mu\,\delta q \qquad \text{(Eq. I.22)}$$

At constant temperature, Eq. I.22 transforms into $\delta\overline{G}^{a} = \mu\,\delta q$, which combined with Eq. I.21 previously differentiated turns into Eq. I.23, which accounts for the dependence of the surface potential on the chemical potential of the condensed phase:

$$\delta\Phi = -q\,\delta\mu \qquad \text{(Eq. I.23)}$$

Considering that the adsorbent behaves as a perfect gas, $\delta\overline{G}^{a} = \mu\,\delta q$, Eq. I.23 can be integrated, thus giving Eq. I.24

$$\frac{\Phi}{RT} = -\int_0^P q\,\delta\mathrm{Ln}(P) = -q_M \int_0^P \theta\,\delta\mathrm{Ln}(P) \qquad \text{(Eq. I.24)}$$

As can be observed from Eq. I.24, $\Phi/RT < 0$ for $\forall\theta \le 1$ and it becomes more negative as $\theta \to 0$. On the other hand, the integral free energy of the adsorbed phase, $\Delta\overline{G}^{a}$ [J kg^{-1}], is defined as the difference between the internal free energy of the adsorbate and the free energy of the adsorbate as a gas phase at standard state, $\boldsymbol{\mu^{o}}$, according to Eq. I.25

$$\Delta\overline{G}^{a} = \overline{G}^{a} - q\,\mu^{o} \ [\mathrm{J\ kg^{-1}}] \qquad \text{(Eq. I.25)}$$

Combining Eq. I.25 with Eq. I.21, Eq. I.26 is obtained

$$\Delta\overline{G}^{a} = q\left(\mu - \mu^{o}\right) + \Phi\,, \qquad \text{(Eq. I.26)}$$

which transforms into Eq. I.27 if the adsorbate is regarded as a perfect gas

$$\Delta\overline{G}^{a} = q\,RT\,Ln\left(\frac{P}{P^{o}}\right) + \Phi\,, \qquad \text{(Eq. I.27)}$$

where $\mathbf{P^o}$ is the vapor saturation pressure [kPa]. The differential free energy, $\mathbf{\Delta\bar{g}^a}$ [J mol^{-1}], can be obtained by differentiating the integral free energy

$$\Delta\bar{g}^{a} = \left.\frac{\partial \Delta G^{a}}{\partial q}\right|_{T} = RT\,Ln\left(\frac{P}{P^{o}}\right) \qquad \text{(Eq. I.28)}$$

I.3.6.2. Mixture adsorption equilibrium in zeolites: thermodynamic consistency

The simplest expression to account for the multicomponent adsorption equilibrium in zeolites is a extended Langmuir-type isotherm, which, for species **i**, takes the form

$$q_i = q_{i,M}\,\frac{K_i\,P_i}{1+\sum_{j=1}^{C} K_j\,P_j} \quad [\text{mol kg}^{-1}] \qquad \text{(Eq. I.29)}$$

For thermodynamic consistency, the saturation loading for all the species must be equal in the Extended Langmuir isotherm (*Sircar, 1991*). This definition implies that different loadings are needed to obtain similar fractional occupancies. According to *Krishna (2001)*, when two species in a mixture have significantly different molecular sizes, size entropy effects tend to favor the adsorption of the smaller species at high loadings. This is the case, for example, for adsorption of methane and n-butane in silicalite-1 (*Kapteijn et al., 2000*). Furthermore, for mixtures of linear and branched alkanes, configurational entropy effects tend to favor the adsorption of linear alkanes because the former molecules pack more efficiently than the latter.

Various approaches have been proposed in the literature to account for thermodynamically consistent models for mixture adsorption. Among them, the Ideal Adsorbed Solution Theory (IAST) developed by *Myers and Prausnitz (1965)* reveals more adequate to describe mixture adsorption and further modifications such as the Real Adsorbed Solution Theory (RAST) (*Costa et al., 1981*) and the Predictive Adsorbed Solution Theory (PRAST) (*Sakuth et al., 1998*) to account for non-ideality of the adsorbate reveal more adequate to describe mixture adsorption. By using either the concepts of spreading pressure (2D) or surface potential (3D), this formalism allows to derive multicomponent adsorption isotherms from unary adsorption isotherms. For solution thermodynamics, the IAS approach

relies on an analogy with the Raoult's Law for vapor-liquid equilibria through Eq. I.30 for microporous adsorbents

$$P\, y_i = P_i^o(\Phi)\gamma_i(\Phi)x_i \quad [\text{kPa}] \qquad \text{(Eq. I.30)}$$

where $\mathbf{y_i}$ and $\mathbf{x_i}$ are the molar fractions of species **i** in the gas and "fluid" phases [-], respectively, $\boldsymbol{\gamma_i(\Phi)}$ is the activity coefficient of species **i** in the "fluid " adsorbate [-], and **P** is the total pressure in the gas phase [kPa]. However, compared to the Raoult's Law, there is a subtle difference in the meaning of $\mathbf{P_i^o}$ [kPa]. In the case of vapor-liquid equilibria, P_i^o is the saturation vapor pressure of species **i** at the temperature of the solution, while $P_i^o(\Phi)$ is the adsorptive saturation pressure (actual saturation vapor pressure) corresponding to the solution temperature and surface potential Φ.

The IAS approach requires the resolution of Eqs. I.30 for all the species in the mixture, which allows the representation of a Y-X equilibrium diagram. Beyond the Y-X equilibrium diagram, a loading diagram is also necessary, which connects the total adsorbed amount, q_i, with the gas (vapor) phase mole fraction of the key species. The following expressions are proposed (Eqs. I.31 and I.32)

$$\frac{1}{q^T} = \sum_{i=1}^{N}\frac{x_i}{q_i^o(\Phi)} + \sum_{i=1}^{C}\left[\frac{\partial \ln\gamma_i(\Phi)}{\partial\Phi}\right] \quad [\text{kg mol}^{-1}] \qquad \text{(Eq. I.31)}$$

$$q_i = x_i\, q^T \qquad \text{(Eq. I.32)}$$

where $\mathbf{q^T}$ is the total loading, $\mathbf{q_i^o(\Phi)}$ is the loading of pure species **i** [mol kg^{-1}] at surface potential Φ [J kg^{-1}], and $\mathbf{q_i}$ is the loading of species **i** for the given mixture. The expression $[\partial \text{Ln}\gamma_i(\Phi)/\partial\Phi]_{T,xi}$ can be approximated in a numerical way by Eq. I.33

$$\left[\frac{\partial \text{Ln}\,\gamma_i(\Phi)}{\partial\Phi}\right]_{T,x_i} = \lim_{x_i\to 0}\frac{\text{Ln}[\gamma_i(\Phi_j)] - \text{Ln}[\gamma_i(\Phi_{j-1})]}{\Phi_j - \Phi_{j-1}}, \qquad \text{(Eq. I.33)}$$

with $\Delta x = x_i(\Phi_j) - x_i(\Phi_{j-1})$.

I.3.6.3. Adsorption measurement

Microcalorimetry (*Dunne et al., 1996; Lee et al., 1997b*), gravimetric (*Sun et al., 1998*) and volumetric uptake (*Li et al., 2001c; Pakseresht et al., 2002*), temperature programmed desorption (*Millot et al., 1999*), tapered oscillating microbalance measurements (TEOM) *(Van den Graaf et al., 1998; Zhu et al., 1998*), chromatography (*Meininghaus and Prins, 2000*), FTIR (*Rege and Yang, 2001*), adsorption-branched porosimetry (*Clark et al., 2004*), and transient permeation (*Gardner et al., 2002*) constitute the most widespread techniques

reported in the literature for measuring gas- and liquid-phase adsorption on zeolite powders. Although all these techniques work well for pure species (unary adsorption), they are difficult to use for mixture adsorption. Furthermore, for liquid mixtures, differentiating between adsorbed molecules and wetting on the outer surface of zeolite crystals is also difficult. The best technique for measuring mixture adsorption in zeolites is gas- or liquid-phase chromatography using an adsorbent column packed with zeolite powder, which has the additional advantage of measuring diffusivities (*Boulicaut et al., 1998; Lin and Ma, 1988*).

Despite the great number of studies concerning the adsorption equilibrium of gases in zeolites, only a few were directed to determine adsorption isotherms of water and alcohols in zeolites. For instance, *Okamoto et al. (2001)* and *Zhu et al. (2005)* measured the pure water adsorption isotherm on zeolite A, respectively, by a volumetric method and by the TEOM technique. *Nayak and Moffat (1988)* and *Lin and Ma (1988)* determined pure alcohol adsorption isotherms on silicalite-1, respectively, by gravimetric uptake and by high performance liquid chromatography (HPLC). Moreover, *Yamazaki and Tsutsumi (1997)* determined adsorption isotherms for pure water, methanol, t-butanol, and n-hexane vapors on mordenite using a gravimetric method, and *Giaya and Thompson (2002)* reported isotherms of several chlorinated species on various zeolites using the TEOM technique. Finally, *Cruz et al. (2004)* measured acetic acid vapor isotherms on zeolites NaX and NaY.

I.3.7. Adsorption kinetics and diffusion in subnanoporous materials

Compared to nanoporous materials (mean pore size >1 nm), where significant mass transfer of adsorbed molecules can occur by surface diffusion or “skating” along the pore wall (*Burggraaf, 1999*), molecules tend to be transferred in subnanoporous materials (mean pore size <1 nm) (e.g., zeolites) by ***surface*** or ***configurational diffusion*** pathways due to their interaction with the potential field of the zeolite walls, except for high temperatures (473 – 773 K), where Knudsen activated diffusion or ballistic pathways are predominant (*Nicholson and Petropoulos, 1973; Bakker et al., 1997; Yoshioka et al., 2001*).

I.3.7.1. Diffusivities in zeolites

Two types of diffusivities (i.e. Fick or transport diffusivities, D [m^2 s^{-1}], and self-diffusivities, D^* [m^2 s^{-1}]) can be measured in zeolites. The fundamental difference between both types of diffusivities relies on the presence of finite gradients. Transport diffusivities are measured under *non-equilibrium* conditions in which finite gradients of loading exist ($\nabla q_T \neq 0$), while self-diffusivities are measured under *equilibrium* conditions ($\nabla q_T = 0$) and involve mass transfer of identical but labeled molecules.

Techniques such as the pulsed-field-gradient nuclear magnetic resonance (PFG NMR) (*Bussai et al., 2002a; Paoli et al., 2002*), quasi-electric neutron scattering (QENS) (*Jobic et al., 1999, 2000, 2003; Paoli et al., 2002*), neutron-spin echo (NSE) (*Jobic et al., 2002, 2003*), chromatography (*Lin et al., 1988*), transient uptake (*Doelle et al., 1981; Nayak and Moffat, 1988; Shah et al., 1988*), constant volume method (*Masuda et al., 1996; Micke et al., 1994*), frequency reponse (*Song et al., 2002*), and transient permeation (*Bowen et al., 2004a,b; Gardner et al., 2002; Zhu et al., 2005*) have been used to measure these diffusivities. The first two techniques consist of equilibrium microscopic methods that measure the self-diffusivity, while the others are non-equilibrium macroscopic methods suitable for measuring transport diffusivities. Self- and transport diffusivities have been also calculated, respectively, by equilibrium molecular dynamics (EMD) (*Bussai et al., 2002b; Krishna, 2000*), and by non-equilibrium molecular dynamics (NEMD) simulations (*Furukawa et al., 2004; Krishna, 2000; Maginn et al., 1993*). In general terms, the self-diffusivities (10^{-10} – 10^{-9} m^2 s^{-1}) tend to agree fairly well with those determined form microscopic methods. However, diffusivities measured with macroscopic methods are often between three and five orders of magnitude lower (10^{-15} – 10^{-12} m^2 s^{-1}).

Transport and self-diffusion in zeolites constitute temperature-dependent processes that take place by a sequence of jumps between regions of low potential energy or sites (*Xiao and Wei, 1992; Yoshioka et al., 2001*) (see Figure I.4), which can be described by the Arrhenius equation (Eq. I.34)

$$D^{(*)} = D_0^{(*)} \exp\left(-\frac{E_D^{(*)}}{RT} \right) \qquad \text{(Eq. I.34)}$$

where **D** is the diffusivity [m^2 s^{-1}], $\mathbf{D_o}$ is a pre-exponential factor [m^2 s^{-1}], and $\mathbf{E_D}$ is the activation energy for diffusion [J mol^{-1}]. The asterisk refers implicitly to self-diffusion. To be able to diffuse through a zeolite matrix, the molecules must have enough energy to overcome the potential wells at each adsorption site. Activation energy tends to increase as the kinetic diameter of the molecules approaches the pore size of the zeolite because the number of molecule-wall interactions increase. For instance, *Chloudhary et al. (1992)* reported activation energies for C_4-C_8 alcohols in ZSM-5 (pore size: 0.53 x 0.55 and 0.51 x 0.56 nm) that ranged from +16 kJ mol^{-1} for C_4 to +41 kJ mol^{-1} for C_8 hydrocarbons.

I.3.7.2. Generalized Maxwell-Stefan diffusional theory: Maxwell-Stefan vs. Fickian (transport) diffusivities

The generalized Maxwell-Stefan theory (GMS) earlier developed by *Krishna (1990)* from multicomponent diffusion on bulk fluids and further applied with great skill by *Krishna*

(1993), Krishna and Van den Broeke (1995) and *Krishna and Wesselingh (1997)* provides an adequate basis for the description of multicomponent mass transfer of adsorbed species in zeolites when surface diffusion along the surface within the adsorbent pores is the rate limiting process. Since the size of the permeating molecules are on the same order as that of the micropores, the GMS theory conventionally assumes that movement of a species is caused by a driving force which is balanced by the friction experienced from each other and its surroundings (*Krishna and Wesselingh, 1997*). Taking the isothermal gradient of chemical potential for each species i, $-\nabla_T \mu_i$ [J mol^{-1} m^{-1}], as the driving force, treating vacancy sites as active species, and using the mechanistic model depicted in Figure I.6a as a theoretical guideline, the general form of the GMS equations applied to surface diffusion is given by Eq. I.35

$$-\rho_p \frac{q_i}{RT} \nabla_T \mu_i = \sum_{\substack{j=1 \\ j\neq i}}^{C} \frac{\left(q_j N_i^S - q_i N_j^S \right)}{q_{M,j} Đ_{ij}^S} + \frac{N_i^S}{Đ_{iV}^S} \qquad i, j = 1,2,\ldots, C \qquad \text{(Eq. I.35)}$$

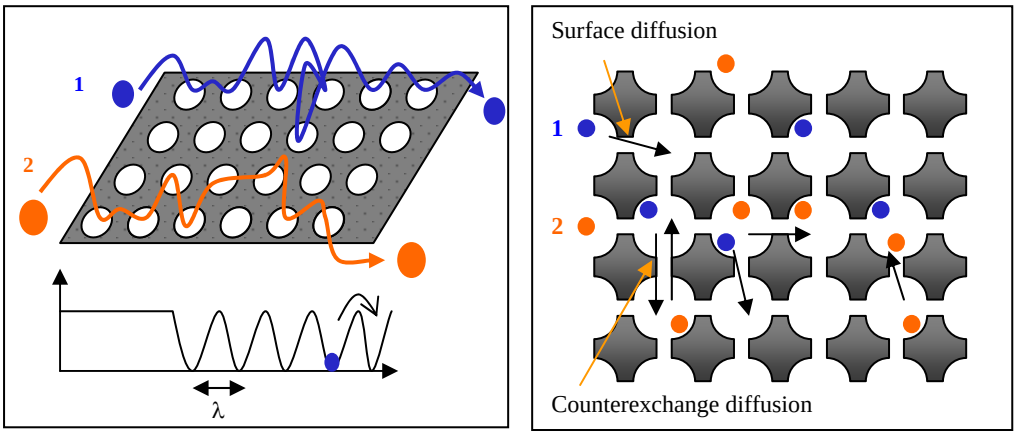

Figure I.6: (a) Conceptual model for surface diffusion of adsorbed species 1 and 2; (b) Diffusion processes within a zeolite framework.

where $\mathbf{q_i}$ and $\mathbf{q_j}$ are the molar loadings of species **i** and **j** [mol kg^{-1}], respectively, and N_i^S and N_j^S are the surface fluxes of species **i** and **j** [mol m^{-2} s^{-1}], respectively. The first term on the right-hand side in Eq. I.35 reflects the friction exerted between adsorbed molecules, while the second one represents the friction between a molecule and the pore wall. Both interactions can be modeled, respectively, by means of *MS counterexchange diffusivities*, $\mathbf{Đ_{ij}^S}$ [m^2 s^{-1}], and *MS surface or "jump" diffusivities*, $\mathbf{Đ_i^S}$ [m^2 s^{-1}] (see Figure I.6b). For cage-type topologies (3D) with high connectivities (e.g., LTA) and for pore-type zeolites (2D) under the situation of ***single-file diffusion*** (i.e. $d_{m,i} + d_{m,j} < \bar{d}_p$) (e.g., i-butane in MFI-type zeolites) (see Figure I.7), the counterexchange coefficient $Đ_{ij}^S$ can be expected to be high (i.e. $Đ_{ij}^S \rightarrow \infty$), which implies

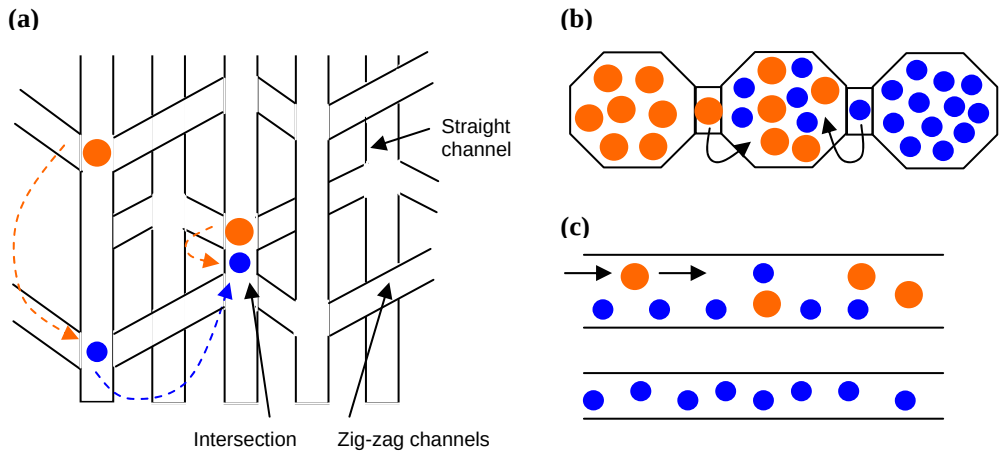

Figure I.7: Pictorial representation of the molecular jumps in: (a) Intersecting channel structures (MFI), (b) cages separated by windows (LTA, FAU, CHA) and (c) single-file diffusion in one-dimensional channels (MOR).

that the mobility of adsorbed species **i** is not expected to contribute to the mobility of **j** (*Krishna, 1990; Van den Broeke, 1995*). For this particular situation, the first term on the right-hand in Eq. I.34 vanishes. It should be noted that the MS formalism involves the use of MS diffusivities rather than fickian or transport diffusivities, because surface fluxes are related to chemical potential gradients instead of loading gradients.

I.3.7.3. Dependence of MS surface or "jump" diffusivities with total loading

Mechanistically, the MS surface diffusivity, $Đ_i^S$, can be related to the displacement of the adsorbed molecular species, λ [m], and the jump frequency, $\nu(q^T)$ [s^{-1}] by Eq. I.36, which in general can be expected to be dependent on the total molar loading, q^T [mol kg^{-1}] (*Reed and Ehrlich, 1981; Chen and Yang, 1991; Xiao and Wei, 1992*)

$$Đ_i^S\left(q^T\right) = \frac{1}{z}\lambda^2\,\nu_i\left(q^T\right) \qquad \text{(Eq. I.36)}$$

where λ is the average jump distance [m], **z** is the number of nearest neighbor sites [-], and $\nu_i(q^T)$ is the jump frequency of species **i** [s^{-1}]. For weak confinement in the zeolite framework, the jump frequency remains constant, that is $\nu_i(q^T) = \nu_i(0)$ independent of the molar loading, the MS surface diffusivity of species **i**, $Đ_i^S$, is also independent of the molar loading, that is

$$Đ_i^S\left(q^T\right) = \frac{1}{z}\lambda^2\,\nu_i(0) = Đ_i^S(0) \qquad \text{(Eq. I.37)}$$

On the other hand, for strong confinement in the zeolite framework, the jump frequency decreases with the molar loading due to the interactions between the adsorbed species. If it is assumed that a molecule can only migrate between two neigbor sites only if the final one is vacant, the likelihood that this takes place can be expressed by Eq. I.38 (*Xiao and Wei, 1992*)

$$\nu_i\left(q^T\right)=\nu_i(0)q_V \;;\; Đ_i^S(q_T)=\frac{1}{z}\lambda^2\,\nu_i(0)q_V = Đ_i^S(0)q_V \qquad \text{(Eq. I.38)}$$

On the other hand, the coefficients $Đ_{ij}^S$, express the interactions between adsorbates **i** and **j**. Krishna suggested the use of the *Vignes (1996)* relationship for the determination of these coeficients (Eq. I.39)

$$Đ_{ij}^S(q_T)=\left[Đ_i^S(0)\right]^{\theta_i/(\theta_i+\theta_j)}\left[Đ_j^S(0)\right]^{\theta_j/(\theta_i+\theta_j)} \qquad \text{(Eq. I.39)}$$

It should be noted that the MS surface diffusivities at zero coverage, $Đ_i^S(0)$ are usually assumed to be temperature-dependent according to the Arrhenius equation analogous to Eq. I.34 (Eq. I.40) (*Reed and Ehrlich, 1981; Shelekhin et al., 1995*)

$$Đ_i^S(0)=A_i^S\exp\left(-\frac{E_i^S}{RT}\right), \qquad \text{(Eq. I.40)}$$

where $\mathbf{A_i^S}$ is the pre-exponental factor [$m^2\ s^{-1}$] and $\mathbf{E_i^S}$ is the activation energy [kJ mol^{-1}].

I.3.7.4. Equations for unary and multicomponent mass transfer in zeolites

Assuming equilibrium between the surface and the bulk fluid, the following relationship for the surface chemical potential, μ_i [J mol^{-1}], can be written (Eq. I.41)

$$\mu_i=\mu_i^o+RT\,Ln(f_i), \qquad \text{(Eq. I.41)}$$

where μ_i^o is the chemical potential at the chosen standard state [J mol^{-1}] and $\mathbf{f_i}$ is the fugacity of species **i** in the bulk fluid mixture [kPa]. For not too high system pressures, the partial pressure, P_i [kPa], can be used in place of fugacities (i.e. $f_i = P_i$). The surface chemical potential gradients may be expressed in terms of the gradients of molar loadings by introduction of the matrix of thermodynamic factors, Γ_{ij} (Eqs. I.27 and I.28) (*Krishna, 1990*)

$$\frac{q_i}{RT}\nabla\mu_i=\sum_{j=1}^{N}\Gamma_{ij}\frac{q_{i,M}}{q_{j,M}}\nabla q_j \quad \text{where } \Gamma_{ij}\equiv q_i\left(\frac{q_{j,M}}{q_{i,M}}\right)\frac{\partial Ln(P_i)}{\partial q_j} \quad i,j = 1,2,\ldots, C$$

(Eqs. I.42 and I.43)

The form of the thermodynamic factors is determined by the form of the multicomponent adsorption isotherm chosen to relate molar loadings, q_i [mol kg^{-1}], to the partial pressure, P_i. In most of the studies reported in the literature, the Langmuir isotherm (either single- or dual-site) is usually chosen to account for the unary and multicomponent adsorption (Eqs. I.7 and I.9) (*Van den Broeke and Krishna, 1995; Bakker et al., 1996; Van den Graaf et al., 1999; Millot et al., 2000*). On the other hand, *Kapteijn et al. (2000)* derived expressions to account for multicomponent adsorption for species with different molar saturation loadings under the IAS approach described in section I.3.6.2. Introducing Eqs. I.42 and I.43 to Eq. I.35 with the Extended Langmuir isotherm, and recasting in n-dimensional matrix notation, Eq. I.44 is obtained

$$-\rho_p\, q_M [\Gamma](\nabla\theta) = [B^S](N^S)\ , \qquad \text{(Eq. I.44)}$$

where the matrix $[B^S]$ includes the elements (Eq. I.45)

$$B^S_{ii} = \frac{1}{Đ^S_i} + \sum_{\substack{j=1\\ j\neq i}}^{N} \frac{\theta_j}{Đ^S_{ij}} \quad \text{and} \quad B^S_{ij(i\neq j)} = -\frac{\theta_i}{Đ^S_{ij}}\ ,\ i,j = 1, 2, \ldots C \qquad \text{(Eq. I.45)}$$

The matrix of fickian or transport diffusivities, $[D^S]$, is defined by Eq. I.46

$$[D^S] = [B^S]^{-1}[\Gamma] \qquad \text{(Eq. I.46)}$$

where $[\Gamma]$ is the matrix of thermodynamic factors. Therefore, Fick or transport diffusivities, $[D^S]$, are composite of diffusive effects, $[B^S]$, and thermodynamic effects, $[\Gamma]$. If the condition $Đ^S_{ij} \to \infty$ is fulfilled, the matrix of fickian diffusivities can be simplified to a n-dimensional diagonal matrix (Eq. I.47)

$$[D^S] = \begin{bmatrix} Đ^S_1 & 0 & 0 & 0 \\ 0 & Đ^S_2 & 0 & 0 \\ 0 & 0 & \ddots & 0 \\ 0 & 0 & 0 & Đ^S_C \end{bmatrix} [\Gamma] = [Đ^S][\Gamma\ ]\text{,} \qquad \text{(Eq. I.47)}$$

which for the mass transfer of a single species, allows to obtain the so-called ***Darken equation*** (*Van den Broeke and Krishna, 1995*) (Eq. I.48)

$$D^S_i = \frac{Đ^S_i}{1-\theta_i} \qquad \text{(Eq. I.48)}$$

Furthermore, according to *Krishna (2002)*, MS surface diffusivities can be also related to self-diffusivities by Eq. I.49

$$D^*_i = \frac{Đ^S_i}{1+F\,\theta_i} \qquad \text{(Eq. I.49)}$$

where **F** is a factor that depends on the zeolite topology. According to Eqs. I.48 and I.49, when the adsorbate loading is low, the thermodynamic factors tend to unity, thus indicating that for nearly ideal systems Fickian, MS and self-diffusivities agree (i.e. $D_i^S = Đ_i^S = D_i^*$).

I.4. ZEOLITE MEMBRANES: AN OVERVIEW

Among microporous inorganic membranes, zeolite membranes constitute a promising technology not only for separation processes and catalytic membrane reactors (*Coronas and Santamaria, 1999; Matsukata and Kikuchi, 1997; Tavolaro and Drioli, 1999*), but also for more incipient fields, such as microreactors, sensors, electrodes, optoelectronic devices and artificial organs (*Coronas and Santamaria, 2004a,b*). These processes take advantage of the unique properties of zeolites (e.g., highly crystalline ordered structure, molecular-sized pores, thermal stability and resistance to harsh environments, to swelling and to microbiological attack) when used in a film-like configuration. These attributes make zeolite membranes attractive alternatives for separating mixtures whose components display adsorption or size differences, but are difficult to perform using either polymeric membranes or other conventional separation techniques. In the last 15 years, there has been an intense development in the field of zeolite membranes, as can be observed from the increased number of patents and scientific papers related to these kind of membranes (*Caro et al., 2000*). By now, more than 14 types of zeolite membranes have been successfully synthesized at a laboratory scale.

I.4.1. Preparation of zeolite membranes

The synthesis procedures of zeolite membranes have evolved in recent years in order to improve their reproducibility. Compared to other inorganic membranes, the sol-gel method is not usually used for the synthesis of zeolite membranes. The first application of zeolites in the form of a membrane was reported by *Kemp and Paul (1974)* as zeolite-filled membranes and later by *Gao et al. (1996)*, where zeolite crystals were embedded in a support, usually polymeric. Further studies focused on embedding inorganic supports with zeolite crystals in order to improve both thermal and chemical stability (*Kölsch et al., 1994*).

Since the 90s, most synthesis methods are based on the crystallization of zeolite layers under controlled pressure and temperature conditions from a gel that provides the Si and Al zeolite precursors that are required to grow the zeolite layers. Among them, most of the zeolite membranes reported have been prepared onto or into a porous substrate (composite or supported membranes). The different synthesis strategies used up to now for zeolite membrane preparation are summarized in Figure I.8. These processes can be listed as follows:

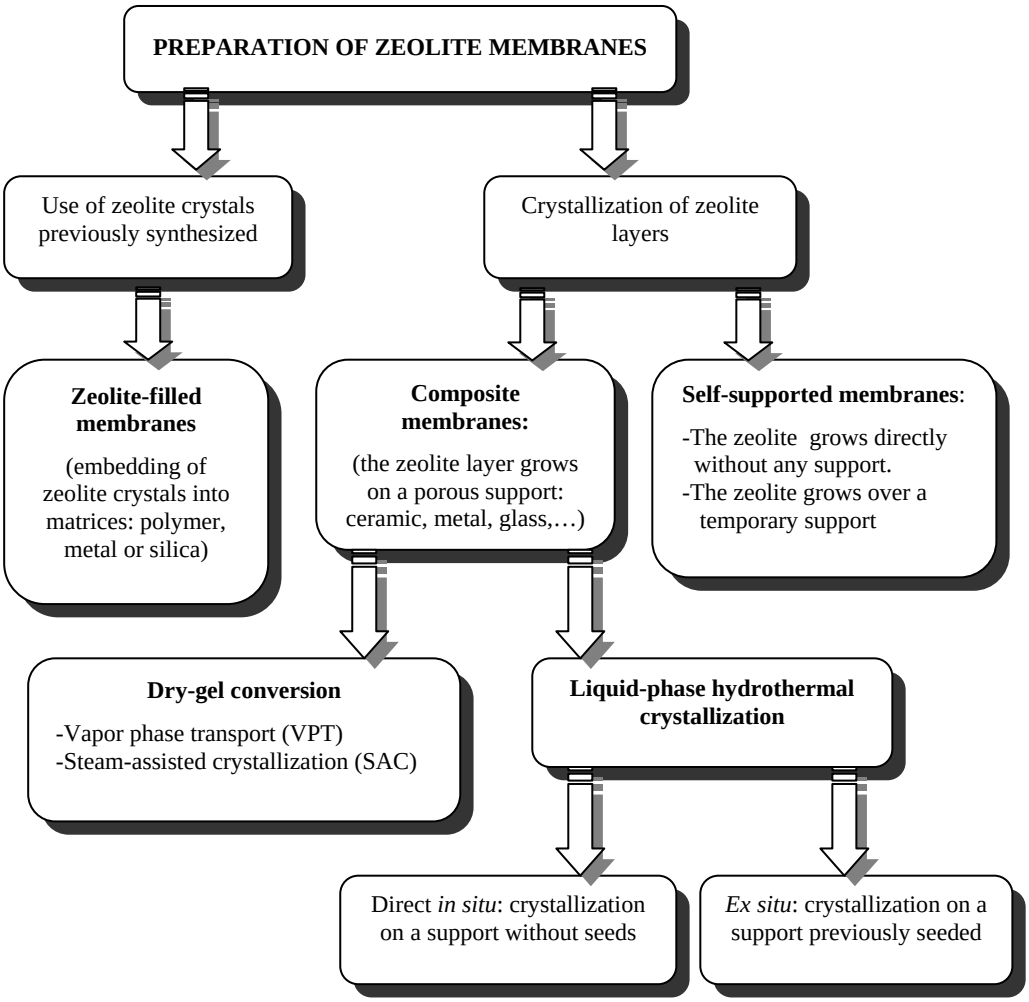

Figure I.8: Synthesis strategies for zeolite membranes preparation.

I.4.1.1. Self-supported membranes

Self-supported membranes are prepared without a support or onto a temporary support (Teflon, polyethylene, glass, cellulose,…), which is thermally or mechanically removed after the synthesis of the zeolite layer. There are only few examples of zeolite membranes prepared with this procedure, because the membranes do not show enough mechanical resistance. Several examples of this membranes have been reported by *Myatt et al. (1992)* and *Lee and Dutta (2000)*. These membranes have practically no applications due to their small dimensions and their low mechanical resistance.

I.4.1.2. Composite or supported membranes

Most of the zeolite layers are prepared onto a meso- or macroporous inorganic support (usually α,γ-alumina, titania and stainless steel), which provides the required mechanical resistance to the system and allows the growth of a selective zeolite layer. The support can present different shapes (flat, tubular,…) and can be made of several materials (α, γ-alumina, silica,titania, zirconia, stainless steel). The first patent on supported zeolite membranes was reported by *Suzuki et al. (1987)*. From the point of view of the industrial application, tubular membranes are more suitable than flat, because tubes are easier to scale up (implemented as multichannel modules). However, for laboratory-scale applications, the synthesis of good quality zeolite membranes onto a tubular support is usually found to be more difficult than on a porous disk due to the following reasons (*Coronas and Santamaria, 1999*):

- The area is usually smaller in flat supports, which contributes to decrease the likelihood of defects.
- In the hydrothermal synthesis, tubular supports are often placed vertically in the autoclave filled with the synthesis gel, the amount of which must be in sufficient excess to avoid local depletion of the nutrients.
- With flat supports, the crystal nuclei formed in the bulk of the solution precipitate onto the support, which facilitates the formation of the zeolite layer, something difficult to be achieved with vertical support tubes.

The aim of composite membrane synthesis is the preparation of continuous and defect-free zeolite layers onto a support with good thermal, chemical and structural properties, able to control and limit the permeation of species only on the grounds of their sieving or adsorption characteristics. Two major synthesis processes for composite zeolite membranes have been reported in the literature: ***dry-gel conversion*** (section I.4.1.2.1) and ***liquid-phase hydrothermal synthesis*** (section I.4.1.2.2). In general terms, the concentration of synthesis gel/solution is higher in dry-gel conversion and lower in seeded growth method. Accordingly, the rate of nucleation is higher in dry-gel conversion, while lower in seeded growth method.

I.4.1.2.1. Dry-gel method (DGM)

This method is based on the deposition of a layer of the Si and Al precursors as a dry aluminosilicate gel onto the support using sol-gel techniques (*dip coating*) and further zeolitization of this gel under the presence of vapors (*Matsukata et al., 1994*). This has the additional advantage of optimizing the waste reactants and the avoidance of crystal nucleation in the homogeneous phase. With this general approach, two routes can be distinguished,

namely the ***Vapor Phase Transport*** method (VPT) (when the organic SDAs are not included in the dry parent gel) and the ***Steam-Assisted Crystallization*** (SAC) where the dry gel contains the SDAs, generally quaternary amines, and only steam is supplied from the vapor phase.

Xu et al. (1990) reported for the first time the conversion of a dry aluminosilicate gel into MFI type zeolite by putting the gel into contact with water and amine vapors. *Dong et al. (1992)* and *Alfaro et al. (2001)*, using a similar procedure, prepared MFI zeolite membranes onto both alumina and stainless steel supports. Similarly, zeolite membranes were also prepared by vapor phase regrowth of colloidal MFI type zeolite particles deposited on disks (*Tsay and Chiang, 2000*), or by liquid phase hydrothermal treatment of a dry gel barrier previously incorporated onto an alumina support (*Zhao et al., 2000b*). In addition to MFI, various other types of zeolites, such as FER, MOR and FAU and high silica beta have been synthesized as membranes by means of the dry-gel conversion method *(Matsukata et al., 1994,1997,1999; Nishiyama et al., 1995). Nishiyama et al. (1996,1997)* reported that the structure of the dry gel affected the final zeolite membrane structure. They pointed out the importance in preparing dense dry gel layers to promote the formation of compact zeolite membranes. For this purpose, they revealed that pH was the key parameter.

I.4.1.2.2. Liquid-phase hydrothermal synthesis

Liquid-phase hydrothermal synthesis constitutes the most widely used preparation method of zeolite membranes, in which the porous support is immersed into an alkaline synthesis solution or hydrogel that contains the silica, alumina and sodium nutrients together with an optional SDA (*Coronas and Santamaria, 1999*), and the membrane is synthesized under atmospheric or autogenous pressure in one or more synthesis cycles. As can be seen in Figure I.8, the method can be carried out either with a previous seeding of the support with zeolite crystals (***seeded hydrothermal synthesis*** or ***secondary growth method***), or without a previous seeding step (***direct in situ crystallization***). Some liquid-phase hydrothermal synthesis conditions reported in the literature either with or without a previous seeding step for the preparation of several types of zeolite membranes are summarized in Tables I.8-I.11.

Direct in situ crystallization

Direct in situ crystallization constitutes the most used zeolite membrane synthesis method. In this process, zeolite layers are grown on a porous support via the formation of an amorphous gel layer that promotes spontaneous heterogeneous nucleation and further growth of zeolite crystals when the support is immersed into the synthesis solution (see Figure I.9a). In many cases, zeolite membranes are prepared under similar conditions as zeolite powder.

Table I.8: Conditions for zeolite NaA membrane preparation by liquid-phase hydrothermal synthesis

Reactor Configuration[*]	*Composition of the synthesis solution (Al_2O_3 : SiO_2 : Na_2O : H_2O : templates)*	*T [K]*	*Time [h] / Cycles*	*Support*	*Seeding technique*	*Seed size [μm]*	*References*
Continuous (AC) (1.5-4 mL min^{-1})	1 : 1.8 : 3.9: 273 : 0	353-363	7 / 1	TiO_2 inner tube	Brush seeding	2	**Pera-Titus et al. (2006b) (This study)**
Semi-continuous (AC) (1/4-1/25 min^{-1})	1 : 1.8 : 3.9: 273 : 0	363-373	5 / 1-2	α-Al_2O_3 inner tube/ outer tube	Brush seeding C-F filtration	2	**Pera-Titus et al. (2006a) (This study)**
Semi-continuous (AC) (1/13-1/25 min^{-1})	1 : 1.8 : 3.9: 273 : 0	363	5 / 1	α-Al_2O_3 outer tube	Rubbing	1	Pina et al. (2004)
Centrifugal field (VS) (100 r.p.m)	1 : 2 : 2 : 120-400 : 0	363-373	3 / 2-4	α-Al_2O_3 inner tube	C-F filtration	2, 4	**Pera-Titus et al. (2005) (This study)**
Centrifugal field (VS) (520-2520 r.p.m)	1 : 1.8 : 3.6 : 270 : 0	373	3 / 2-3		Brush seeding	1	Tiscareño-Lechuga et al. (2003)
Dynamic (AC)[2] (rot. 75 r.p.m)	1 : 5 : 55.1 : 1004.7 : 0	323	48 / 1	ZrO_2 / C sheet	-	-	Jafar and Budd (1997)
Static (VS)	1 : 2 : 3 : 200 : 0	363	16-24 / 1-3	α-Al_2O_3 disk	Dip coating	1	Xu et al. (2005)
	1 : 5 : 50 : 1000 : 0	333	24 / 1	α-Al_2O_3 outer tube	C-F filtration	0.3-3.0	Huang et al. (2004)
	1 : 2 : 3 : 200 : 0	363	24 / 1	hollow fiber	-	-	Xu et al. (2004)
	1 : 4.4 : 41.9 : 833.3	353	4 / 1	TiO_2 disk	UV (32 W)	-	Van den Berg et al. (2003b)
	1 : 5 : 50 : 1000 : 0	363	1-6 / 1	α-Al_2O_3 disk	Dip coating	1	Xu et al. (2001b)
	1 : 2 : 2 : 120 : 0	373	3.5 / 1	mullite, α-Al_2O_3 outer tubes	-	1	Kondo et al. (1997)

Table I.8 (to be continued)

Reactor Configuration	*Composition of the synthesis solution (Al_2O_3 : SiO_2 : Na_2O : H_2O : templates)*	*T [K]*	*Time [h] / Cycles*	*Support*	*Seeding Technique*	*Seed size [μm]*	*References*
Static (Vessel equipped with a distiller)	1 : 2 : 2 : 80-144 : 0	353-373	3-6 / 1	α-Al_2O_3 outer tube	Rubbing Dip coating	200 mesh	Okamoto et al. (2001)
Static (Vessel-MW) [1]	1 : 2 : 3 : 200 : 0	363	5-40 min / 1		Rubbing	NA	Chen et al. (2004)
	1 : 5 : 50 : 1000 : 0	363	15 min / 1	α-Al_2O_3 disk	Rubbing	NA	Xu et al. (2001a)
	1 : 0.85 : 3 : 200 : 0	250 W	15-20 min / 1		-	-	Han et al. (1999)
Static (AC) [2]	1 : 2 : 50 : 5000 : 0	353	5 / 1 [3]	α-Al_2O_3 / SS outer tubes	Rubbing C-F filtration	1	Moron et al. (2002)
	1 : 9 : 80 : 5000 : 0	353	5 / 1	α-Al_2O_3 disk	Rubbing Dip coating	0.7	Kumakiri et al. (1999)

[*] Notation: AC (Autoclave); VS (Vessel open to the atmosphere); NA (Not available)

[1] Electric frequency: 2450 MHz

[2] Autogeneous pressure

[3] After the synthesis of the membrane, Pd was deposited by CVD

Table I.9: Conditions for zeolite X,Y membrane by hydrothermal synthesis (in situ and secondary growth)

Reactor Configuration	*Composition of the synthesis solution (Al_2O_3 : SiO_2 : Na_2O : H_2O : templates)*	*T [K]*	*Time [h] / Cycles*	*Support*	*Seeding technique*	*Seed size [μm]*	*References*
Static (VS)	1 : 10.6 : 14 : 900 : 0	373	6 / 1	γ-Al_2O_3 outer tube	Rubbing	3	Li et al. (2005)
	1 : 3 : 4.2 : 150 : 0	373	6 / 1	α-Al_2O_3 outer tube	Dip coating	3	Li et al. (2001a)
	1 : 9 : 80 : 5000 : 0	353	5 / 1	α-Al_2O_3 disk	Rubbing	0.5	Kumakiri et al. (1999)
Static (VS equipped with a distiller)	1 : 25 : 22 : 660-1100	363-383	5-8 / 1	α-Al_2O_3 outer tube	Dip coating	NA	Kita et al. (2001)
	1 : 10 : 40 : 840 : 0	373-393	3-10 / 1	α-Al_2O_3 outer tube	-	-	Kita et al. (1997)
Static (AC)	1 : 10.7 : 18.8 : 850 : 0	358-378	3-24 / 1	α-Al_2O_3 disk	Dip coating	1.0-1.5	Gu et al. (2005)
	1 : 1.87 : 4.17 : 460 : 10 (TEA [2])	358	2-3 / 1	α-Al_2O_3 disk	Dip coating	200 nm	Nikolakis et al. (2001)
	1 : 12.8 : 17 : 975 : 0 [1]	363	24 / 1	α-Al_2O_3 outer tube	Rubbing	200 mesh	Kusakabe et al. (1998)
	1 : 10 : 14 : 798 : 0	363	6-24 / 1	α-Al_2O_3 outer tube	Rubbing	200 mesh	Kusakabe et al. (1997)

[*] Notation: AC (Autoclave); VS (Vessel open to the atmosphere); NA (Not available)

[1] Membranes further exchanged to Li, K, Mg, Ca, Ba form at 353 K for 4 h at 0.1 M.

[2] TEA: Triethanolammonium

Table I.10: Conditions for mordenite membrane preparation by hydrothermal synthesis (in situ and secondary growth)

Reactor Configuration	*Composition of the synthesis solution (Al_2O_3 : SiO_2 : Na_2O : H_2O : templates)*	*T [K]*	*Time [h] / Cycles*	*Support*	*Seeding technique*	*Seed size [μm]*	*References*
Static (AC) [1]	1 : 240 : 67 : 2933 : 0	453	2-4 / 1	α-Al_2O_3 outer tube	Dip coating	NA	Li et al. (2003)
	1 : 40 : 15.2 : 3200 : 0	453	8-24 / 1	α-Al_2O_3 outer tube	Rubbing	3	Navajas et al. (2002)
	1 : 40 : 15.2 : 1600 : 0	453	8-24 / 1	α-Al_2O_3 outer tube	Dip coating	NA	Lin et al. (2000)
	1 : 25-43 : 3.6-11.4 : 1250 : 3 (TEAOH [2])	423-443	4-5 days / 1 [3]	α-Al_2O_3 outer tube	-	-	Tavolaro et al (2000)
	1 : 81 : 17 : 2080 : 40 (TEAOH [2])	443	21-23 / 1 8-15 / 1	α-Al_2O_3 outer tube	-	-	Piera et al. (1998)

[*] Notation: AC (Autoclave); NA (Not available)

[1] Autogeneous pressure

[2] TEAOH: Tetraethylammonium hydroxide

[3] Membrane calcined at 843 K

Table I.11: Conditions for MFI type (silicalite-1 and ZSM-5) membrane preparation by hydrothermal synthesis (in situ and secondary growth). The membranes prepared by the secondary growth method were subjected to a prior seeding process by dip coating. All the synthesis processes were carried out at autogenous pressure.

Reactor Configuration	*Composition of the synthesis solution (Al_2O_3 : SiO_2 : Na_2O : H_2O : templates)*	*T [K]*	*Time [h] / Cycles*	*Calcination Conditions*	*Support*	*Seed size [μm]* [6,7]	*References*
Continuous (AC) (0.25 cm min^{-1})	0 : 1 : 0.018 : 85 : 0	423	72 / 1	673 K – 1 h	α-Al_2O_3 outer tube	NA	Richter et al. (2003)
Static (AC) [1]	0 : 4.5 : 0.5 : 1000.5 : 1 (TPABr [3]) 0 : 0.32 : 165 : 1 (TPAOH [2])	423-448	2-15 / 1	753 – 8 h	SS grids (2-5 mm opening sizes)	100 nm	Lopez et al. (2005)
	0 : 40 : 0 : 16800 : 12 (TPAOH [2]) : 40 g silicalite	423	8-15 / Several	713 K – 8 h	SS disks	111 nm	Arruebo et al. (2001)
	0 : 1 : 0.09 : 11.4 : 0.244 (TPAOH [2])	418-458	12 / 1	673 K – 20 h	mullite, α-Al_2O_3 and SS outer tube	1-3	Lin et al. (2001)
	1 : 100 : 28 : 4000 : 0	453	12-24 / 1	-	α-Al_2O_3 disk	100 nm	Noack et al. (2000)
	0 : 20 : 7 : 1953 : 3 (TPABr [3])	383-423	4-16 / 1	723-773 K – 10 h	α-Al_2O_3 disk	0.4, 2	Lai and Gavalas (1998)
	1 : 240 : 80 : 22920 : 50 (TPAOH [2])	443	15-24 (1^{st}) 8-17 (2^{nd})	753 – 8 h	α,γ-Al_2O_3 and SS inner tubes	-	Coronas et al. (1998)
	0 : 1 : 0.053 : 14.2 : 0.15 (TPABr)	371-458	0.7-6 days/1	673 K – 20 h	SS disk	-	Bakker et al. (1996)
	0.005 : 6 : 2 : 573 : 1 (TPABr [3]) 0.105 : 21 : 1.605 : 988.5 : 1 (TPABr [3])	443	15-24 / 1	753 K – 8 h	α,γ-Al_2O_3 outer tube	-	Bai et al. (1995)
	0 : 1 : 0.05 : 80 : 0.1 (TPABr [3])	443	48 / 1	773 K – 20 h	SS disk	-	Sano et al. (1995)

[*] Notation: AC (Autoclave); VS (Vessel open to the atmosphere); NA (Not available)

[1] Autogeneous pressure
[2] TPAOH: Tetrapropylammonium hydroxide
[3] TPABr: Tetrapropylammonium bromide

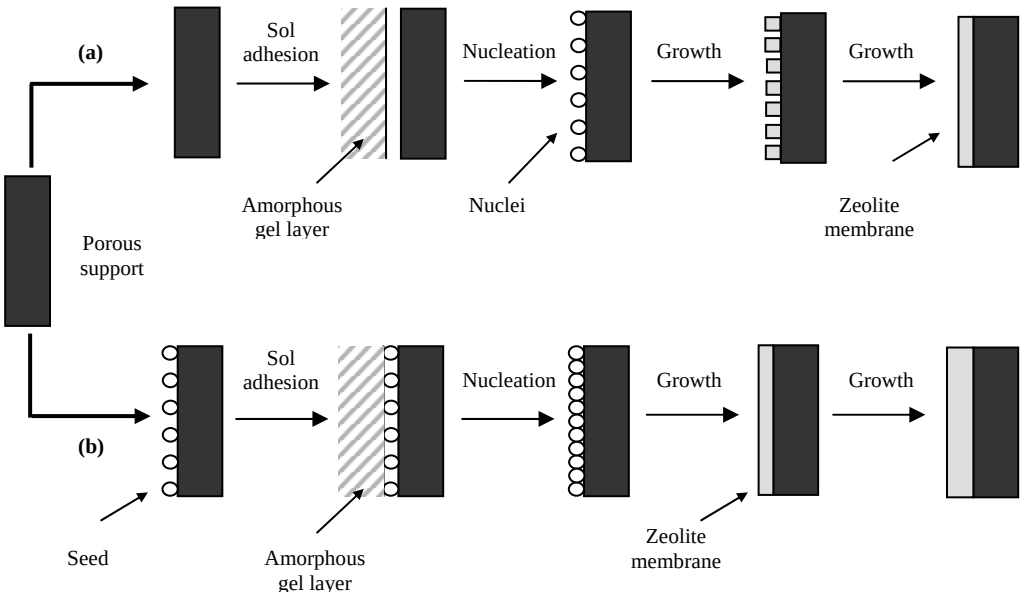

Figure I.9: Comparison of the formation mechanisms of zeolite NaA membranes on porous supports. (a) without and (b) with the aid of seeds

However, the optimal conditions for the synthesis of zeolite membranes are much limited than powder synthesis, and therefore many efforts have been done to screen and optimize the synthesis conditions. It should be noted that both nucleation and growth processes can also take place in the homogeneous phase. As a result, the synthesized nuclei can be transferred and retained onto the support and then the reproducibility of the layer can be reduced. Moreover, the presence of a support introduces a number of new factors that make the synthesis more difficult to reproduce, among which:

- The mechanism of nucleation changes because the surface of the solid provides nucleation sites that are not present in homogeneous synthesis.
- The support itself might dissolve in the synthesis gel due to its alkalinity and therefore change its composition.

Because the support itself can selectively restrict the diffusion of the gel components, synthesis inside the support pores might take place with a composition different from that of the liquid bulk. Additionally, this imposes spatial constraints on crystal growth. On the other hand, in addition to the aspects above outlined, after a certain period of synthesis time, the zeolite layer itself might suffer from dissolution processes, which might favor the local formation of other types of zeolites. For instance, zeolite NaA membranes synthesized from

clear solution tend to dissolve after 3 h of synthesis at 363 K, and other types of zeolites begin to nucleate thereafter. The nucleation rate of zeolite NaX is related to the concentration of the mono-silicate and dimeric-silicate ions. The mono-silicate and dimeric-silicate ions formed by the dissolution of zeolite NaA favor the formation of other types of zeolites.

High silica MFI type zeolite membranes occupy most part of the reported zeolite membranes prepared by direct in situ crystallization. MFI type zeolite membranes are usually synthesized in an autoclave at 443-473 K under autogeneous pressure (see Table I.11). To remove templates, the membranes are usually calcined at 673-823 K after hydrothermal synthesis, which might result in the formation of cracks or defects in the zeolite layers. On the other hand, LTA and FAU type membranes are usually prepared at 343-373 K under atmospheric pressure, and templates are not necessary. On the other hand, in order to reduce synthesis times, several authors have reported recently the preparation of zeolite A membranes by hydrothermal treatment with microwave (MW) heating (see Table I.8). It is well-known that, irrespective of the type of zeolite, MW heating reduces dramatically the synthesis time of zeolite powder (*Slangen et al., 1997*). For instance, while several hours are needed to crystallize zeolite A by conventional liquid-phase hydrothermal synthesis, only ca. 10 min are needed by MW heating.

Seeded hydrothermal synthesis (secondary growth method)

It is well-known in powder zeolite synthesis that seed crystals grow from the beginning of the synthesis time, while an induction period is observed for nucleation (see section I.3.4), because both nucleation and growth processes become decoupled. For the particular case of zeolite layers, the seeding of the support was reported to be an effective approach to improve the quality and reproducibility of membrane synthesis (*Boudreau et al., 1999; Bronic et al., 1999; Chau et al., 2000*). This method involves two subsequent steps: (1) seeding of the surface of the support with zeolite seed crystals and (2) growth of the zeolite seeds by hydrothermal synthesis (see Figure I.8b). Since the concentration needed for secondary growth is lower than that required for direct in situ hydrothermal synthesis, further nucleation is strongly reduced and almost all the crystal growth takes place over the existing crystal seeds. By controlling the composition and concentration of the secondary growth gel, the crystallization of undesired zeolite phases and the dissolution of the support can be avoided, and the rate and direction of crystal growth can, to a certain extent, be controlled. The most popular seeding processes reported in the literature are the following ones:

- ***Rubbing of zeolite powder***: It is based on a manual deposition of zeolite crystals as powder onto the surface of the support. The problem of the method is based on its simplicity: it lacks of reproducibility, often yielding aggregates of crystals rather than

a smooth coverage of seeded particles, and it cannot be used to seed the inner side surface of tubular supports. This method has been widely used in the preparation of zeolite NaA and mordenite membranes (*Kondo et al., 1997; Aoki et al., 1998; Casado et al., 2000; Navajas et al., 2002*).

- ***Brush seeding of zeolite powder*** : The process is similar to the former, but now the zeolite seeds are rubbed on the inner side of tubular supports by using a test-tube brush. This technique also lacks reproducibility and yields aggregates of crystals. Brush-seeding has been used for the synthesis of inner-side tubular zeolite NaA and zeolites NaX and NaY membranes (*Kita et al., 2000; Li et al., 2001a,b; Tiscareño-Lechuga et al., 2003; Pera-Titus et al., 2006a-b*).

- ***Dip coating***: The supports are seeded with crystals (around 100 nm) from a colloidal suspension. The control of pH and rate of dipping allows to synthesize continuous and densely packed zeolite layers. Several zeolite membranes have been prepared using this seeding method (*Lovallo and Tsapatsis, 1996; Lovallo et al., 1996; Boudreau and Tsapatsis, 1997; Lin et al., 2001*). High reproducibilities in the deposition and orientation of crystals can be obtained with this seeding method. The scale-up of the process to supports with larger areas can be easily done. Flat supports, together with both the outer and the inner sides of tubular supports, can be seeded with this process compared to the other seeding methods.

- ***Cross-flux filtration***: The supports are seeded by cross-flow filtration of a suspension of zeolite seeds across a porous solid, and has been employed to prepare the so-called *dynamic membranes* (*Chen et al., 1998; Altman et al., 1999*), especially those based on ZrO_2 and ZrO_2/PAA (PAA = polyacrylic acid) for RO and UF applications. The technique has been applied by different authors for the seeding of either the outer and inner sides of tubular supports (*Kumakiri, 2000; Huang et al., 2004; Pera-Titus et al., 2005*) and allows to obtain a smooth coverage of zeolite crystals depending on the pH of the suspension and the transmembrane pressure.

- ***Laser ablation***: This method is useful to seed small surfaces (up to 1 cm^2) with a high control and reproducibility. *Balkus et al. (1998)* and *Balkus and Scott (1999)* used this technique to prepare oriented UTD-1 membranes onto silicon supports.

Recently, other seeding methods based on electrostatic forces, electrophoresis, and on the activation of titania supports by UV light have also been reported (*Caro et al., 2000; Van den Berg et al., 2003a,b*).

Reactor configuration for zeolite membrane synthesis

Most of zeolite membranes listed in Tables I.8-I.11 have been grown in one or several liquid-phase hydrothermal synthesis cycles (either with or without a previous synthesis step) onto flat supports or onto the outer surface of tubular supports. In case of using disk supports, the typical setting consists of placing them at the bottom or at the top of an autoclave or vessel. On the other hand, to grow zeolite layers onto the outer surface of tubes, the supports are generally placed vertically. Few works can be found in the literature that attempted the growth of zeolite films onto the inner side of tubular supports. This configuration is attractive from the point of view of industrial application, because the zeolite layer is protected from physical damage during handling operations and it makes it easier to compensate the mismatch regarding the expansion coefficients of the zeolite materials and of the support. Moreover, inner-side zeolite synthesis is also desirable in high-area applications involving zeolite membranes grown on bundles of small-bore or capillary supports, since in this case the formation of an inner side membrane is the best method to preserve the individuality of each membrane in the bundle.

However, growing a layer in such a configuration represents a serious challenge due to the restricted accessibility of the synthesis solution components to the lumen of tubular supports, a problem that is likely to become more severe when developing full-size industrial modules rather than in laboratory-scale applications. The concentration of reactants in contact with the growing membrane is lower than in the bulk of the solution, and this may give rise to a variety of problems, such as slower layer growth, formation of undesired crystalline phases and/or amorphous deposits. The problem of reactant depletion can be partially overcome by refreshing the gel inside the lumen of the support. Thus, good quality zeolite layers can be obtained batch wise by rotating the support around its longitudinal axis in the synthesis solution under a low-g centrifugal field (*Tiscareño-Lechuga et al., 2003; Pera-Titus et al., 2005*) (see Table I.10), which not only creates an axial flux that renews the synthesis solution in contact with the membrane, but also helps to drive crystal nuclei of suitable size from the bulk of the solution towards the membrane layer. However, several batch synthesis cycles are usually required to prepare zeolite membranes with suitable properties, which not only makes the process more expensive, but also increases the likelihood of damage to the membrane, since treatments between each cycle (heating/cooling, cleaning, drying,…) can affect the quality of the layers formed and have a negative impact on membrane reproducibility. In addition, the centrifugal field growth method used presents obvious problems regarding its implementation in membrane mass production.

To overcome the main shortcomings in the synthesis of inner-side zeolite membranes, alternative techniques that involve a continuous supply of the reactants to the support surface have been suggested in recent years. Thus, well-intergrowth flat type-A and inner-side tubular

NaA and ZSM-5 membranes were prepared by inducing a forced flux of the synthesis solution towards the membrane (*Kumakiri, 2000; Yamazaki and Tsutsumi, 2000; Arruebo, 2001; Richter et al., 2003; Pera-Titus et al., 2006a-b*). The general advantages of a continuous synthesis system are the following:

- Because of the continuous refreshment of the gel, it improves the quality of the membranes. A higher concentration of nutrients is supplied to the growth interface and convection during the renovation seems also to improve the mass transfer to it.
- It improves the economy of the process, because the number of synthesis cycles for a given synthesis conditions becomes reduced.
- It facilitates the scale-up of the process.

On the other hand, *Pina et al. (2004)* developed a pioneering semi-continuous technique for the preparation of zeolite NaA membranes onto the outer side of tubular supports at 363 K and 10 bar, using a reaction vessel that allowed the synthesis gel around the support to be renewed at regular intervals. The technique was promising, since layer formation could be controlled by adjusting the gel renewal rate. *Pera-Titus et al. (2006a)* extended the semi-continuous technique of *Pina et al. (2004)* to the preparation of zeolite NaA membranes on the inner-side of tubular supports. This technique allowed to overcome the limited accessibility of inner-side growing layers to the reactants by forcing the renewal of the synthesis gel in the lumen of the support, thereby providing a more stable concentration environment during the synthesis and minimizing the undesired effects.

I.4.2. Microstructure of zeolite membranes: non-zeolite pores

Zeolite membranes formed on porous supports usually show randomly oriented polycrystalline structures. Nevertheless, zeolite films with particular spatial orientations have been reported in the literature. *Jansen et al. (1994)* and *Gouzinis et al. (1998)* prepared, respectively, MFI-type zeolite membranes with b- and c-axes perpendicular to the surface of the support, and *Boudreau et al. (1999)* synthesized zeolite NaA membranes with the NaA (001) planes parallel to the surface.

Because of their polycrystalline nature, zeolite layers show the presence of non-zeolite pores or grain boundaries up to 1 nm (*Sano et al., 1994*) in the nearby of two adjacent zeolite crystals. The synthesis procedure, the type of zeolite, and the calcinations conditions affect the number and size of non-zeolite pores. Molecules in non-zeolite pores have different adsorption and diffusion properties from those in zeolite pores. The differences are usually difficult to quantify because of the irregularities in the shape and size of non-zeolite pores. *Nomura et al.*

(2001) assessed different pathways for mass transfer through zeolite pores and grain boundaries when they studied the separation of ethanol from water/ethanol mixtures by vapor permeation after the chemical vapor deposition (CVD) of amorphous silica in the grain boundaries.

Furthermore, the presence of a certain number of large intercrystalline non-zeolite pores or defects (meso- and macroporous) in the zeolite layers, namely pinholes and cracks, is often unavoidable. Other kind of defects such as dome-like have been reported by *Xomeritakis et al. (1999)*, which are formed by a domain of grains that grow larger and to an inclination compared to the rest of the columnar grains that form the dense polycrystalline film. The formation of these defects is attributed to the absence of a close-packed precursor layer underneath the area of the defect, allowing for a less-competitive growth in its neighborhood.

Transport through large non-zeolite pores that are larger than zeolite pores has contributions of both surface and Knudsen diffusion, and might also show viscous flux contribution, which are usually detrimental to membrane selectivity (*Bowen et al., 2002*). Several analyses are used to estimate the contribution of large defects to the permeation through a zeolite layer. For the special case of membranes formed with SDAs, these fill the zeolite pores before calcination and no permeation is allowed though the membranes. Therefore, single gas permeance through a membrane before calcination provides valuable data concerning the role of large defects. Some amount of defects can be formed during the calcination of the membrane, because zeolite crystals might shrink with the removal of the templates. Another method to check the presence of defects is based on measuring the permeation of a molecule larger than zeolite pores. For this purpose, 1,3,5-triisopropylbenzene and SF_6, with kinetic diameters of 0.85 and 0.55 nm, respectively, are usually employed. If the permeance of one of these large molecules is negligible, then the presence of defects larger than their kinetic diameters can be discarded.

Several researchers have devoted their efforts to modeling the influence of non-zeolite pores on the permeation performance of zeolite membranes. In this way, *Nelson et al. (2001)* proposed a model to account for anisotropic MFI type membranes with nanoscopic defects (e.g., grain boundaries). Other researchers described the role of large defects on the performance of zeolite membranes. For instance, *Sanchez et al. (2001)* used the time-lag method to characterize large pores in composite MFI type membranes from experimental He and SF_6 permeance data and *Hanebuth et al. (2005)* developed an algorithm to calculate the contribution of intracrystalline diffusion of adsorbed molecules together with Knudsen diffusion in large pores and grain boundaries to predict experimental H_2 and SF_6 permeance data. Finally, *Pera-Titus et al. (2006e)* proposed a method based on PV data of inner-side tubular zeolite NaA membranes to determine both the mean pore size and the porosity

corresponding to large defects in the zeolite layers. The method revealed useful, because the membranes with highest selectivities towards the separation of ethanol/water mixtures showed the lowest mean pore sizes and/or lowest porosities.

I.4.3. Separations with zeolite membranes based on adsorption properties

In the last 15 years there has been a strong interest in the determination of the ability of zeolite membranes for gas separation and for the separation of liquid mixtures by pervaporation. MFI type membranes have been the target of most investigations for gas separation applications, while zeolite NaA membranes have received much attention for pervaporation purposes due to their strong hydrophilic character.

I.4.3.1. Gas separation

MFI type zeolite membranes have been successfully applied for the separation of isomeric mixtures based on adsorption and diffusion differences, such as those of n-butane from i-butane (*Bai et al., 1995; Kapteijn et al., 1995; Bakker et al., 1996; Arruebo et al. 2001*), n-hexane from i-hexane (*Coronas et al., 1997*) and the isomers of xylene (*Xomeritakis and Tsapatsis, 1999*). Furthermore, well-intergrown A-type zeolite membranes have been used to carry out the separation of H_2/n-butane, H_2/N_2, He/N_2 and O_2/N_2 mixtures, and X- and Y-type have been successfully synthesized for the separation of CO_2/N_2 and CO_2/CH_4 mixtures (*Gu et al., 2005; Kusakabe et al., 1997,1998,1999*). On the other hand, some other gas separation applications can be also found concerning the selective adsorption of one of the species present in a gas mixture in the zeolite pores, thus blocking the diffusion of the others through the membrane. For example, *Piera et al. (1997)* found that the permeation of H_2 or O_2 through mordenite and ZSM-5 membranes was strongly reduced in the presence of water, methanol, ethanol or propanol vapor, which otherwise allowed their separation.

I.4.3.2. Pervaporation of liquid mixtures

Since the beginning of the 90s, a number of studies have been reported in the literature for the separation of liquid mixtures by PV using zeolite membranes. The most outstanding applications of zeolite membranes in this field have been reviewed by *Bowen et al. (2004c)*. The first applications focused on the separation of methanol/MTBE mixtures with silicalite-1 membranes (*Sano et al., 1995*), alcohols from benzene, cyclohexane and MTBE with X- and Y-type zeolite membranes (*Kita et al., 2000*), and benzene from p-xylene mixtures using mordenite membranes (*Nishiyama et al., 1995*).

On the other hand, among the great number of zeolite membranes prepared in a laboratory-scale, those containing low SiO_2/Al_2O_3 ratios (i.e. zeolite NaA, mordenite, and zeolites NaX and NaY) have often been the target of the investigations because they show great ability for the PV dehydration of organic liquid mixtures (e.g., short and long-chain alcohols, DMF, THF,…) (*Kita et al., 1997; Shah et al., 2000; Li et al., 2001b; Okamoto et al., 2001 ; Gallego-Lizon et al., 2002; Navajas et al., 2002 ; Kazemimoghadam et al., 2004; Pina et al., 2004; Pera-Titus et al., 2005,2006a-b*). Zeolite NaA membranes with selectivities up to 40000 and high fluxes for the dehydration of alcohol/water mixtures have been reported in the literature. Currently, commercial PV units based on zeolite NaA membranes are used at industrial level able to dehydrate routinely a variety of solvents (Mitsui Engineering & Shipbuilding Co., LTD, *Morigami et al., 2001*)

Mass-transfer mechanisms in PV by means of zeolite membranes

Despite the great number of studies focusing on zeolite membrane preparation and on their PV performance, hardly any accurate description of the mass transfer through microporous membranes in the PV process has been proposed in the literature. Modeling the PV process is something relevant not only for a proper understanding of the mechanisms involved, but also for the design of PV modules. On the contrary, several models have been presented for polymeric membranes (*Karlsson and Trägårdh, 1993*). The first approach to describe the PV process was proposed by Binning (*Huang, 1991*), who assumed the existence of two phases inside the membrane (***two-film model***), namely, a "solution phase" next to the feed/membrane interface and a "vapor phase" on the other side, so that the permeating molecules experienced their main resistance of permeation only in the vapor phase.

More generally and phenomenologically, the PV process through polymeric membranes is often described by the solution-diffusion model (*Huang, 1991; Wijmans and Baker, 1995*), which involves three successive steps (see Figure I.10): (1) selective solution of the species in the liquid mixture at the feed/membrane interface, (2) diffusion through the membrane, and (3) desorption at the membrane/permeate interface. The diffusion process (2) is usually accounted for by the Fick's First Law with concentration-dependent diffusivities (*Karlsson and Trägårdh, 1993*). For this particular situation, the flux of each species **i** can be described by Eq. I.50

$$N_i^S = Q_i^S \Delta P_i = Q_i^S \left(a_{i,L} P_i^o - P_{i,v} \right) \quad [\text{mol m}^{-2} \text{ s}^{-1}] \qquad \text{(Eq. I.50)}$$

where $\mathbf{Q_i^S}$ is the permeability [mol m^{-2} s^{-1} Pa^{-1}], $\mathbf{a_{i,L}}$ is the activity of species **i** in the liquid feed (retentate) side of the membrane [-], and $\mathbf{P_i^o}$ and $\mathbf{P_{i,v}}$ correspond to the saturation and permeate vapor pressures [kPa], respectively.

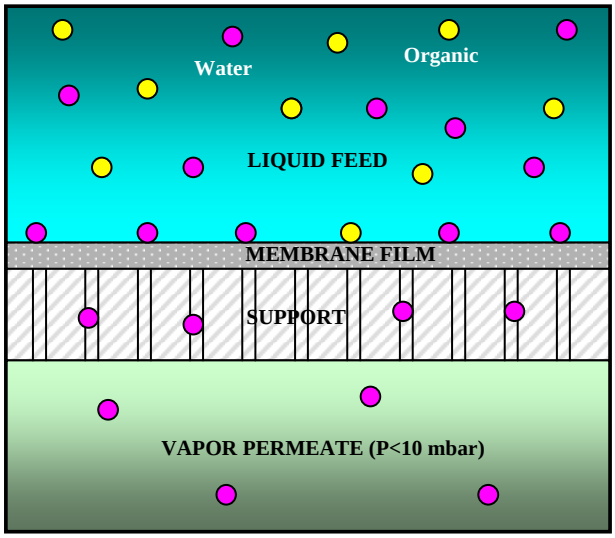

Figure I.10: Solution-diffusion mechanism for PV in a membrane, where the rose species is selectively separated from the yellow one due to its higher affinity to the membrane (*Wijmans and Baker, 1995*)

Recently, *Bowen et al. (2003) and Ortiz et al. (2005)* applied successfully the solution-diffusion model, respectively, for the description of the PV performance of highly hydrophobic Ge-ZSM-5 zeolite membranes (germanium substituted, MFI structure) and for the dehydration of ketonic and THF mixtures (water content 1-8 wt.%) with zeolite NaA membranes. While the former described the diffusion process with constant fickian diffusivities, the latter used an empirically improved version of that model by taking into account a decreasing exponential dependency on the surface coverage or fraction of occupied centers on the adsorbent. However, this model fails to predict the PV performance of zeolite membranes for liquid mixtures with high water content (*Shah et al., 2000*). As it was exposed in section I.3.7, at low temperature, mass transfer through zeolite pores occurs by surface diffusion (*Shah et al., 2000; Nomura et al., 2001*), that is, adsorbed molecules diffuse along the surface of zeolite pores by jumping from site to site, given by the chemical potential gradient along the pores. The dehydration of organic solvents by hydrophilic zeolite membranes usually takes place on the grounds of adsorption differences between water and the solvent.

In an attempt to provide an insight into the mechanisms that govern the PV process, following the general ideas outlined by *Verkerk et al. (2001)* for modeling amorphous silica membranes, *Pera-Titus et al. (2006c)* proposed an adsorption-diffusion model to describe the dehydration performance a zeolite NaA membrane with high selectivity and water flux towards separation of ethanol/water mixtures. In their study, the generalized Maxwell-Stefan

theory (GMS), successfully extended from zeolites (see section I.3.7) and applied for the description of gas permeance through MFI zeolite membranes (see for instance *Krishna, 1990; Van den Broeke, 1995; Van den Broeke and Krishna, 1995; Krishna and Wesselingh, 1997; Millot et al., 2000*), was also used to describe the PV process in order to account for the observed selective water removal.

I.4.3.3. Zeolite membrane reactors

One of the potential applications of zeolite membranes that has received much attention in the last years involves their application in membrane reactors. Most of the studies reported in the literature concern the application of membrane reactors in the field of biotechnology, where the membranes are used for enzyme immobilization. In addition, in the past years there has been an increasing interest in the survey of applications of inorganic membrane reactors to carry out dehydrogenations (*Itoh and Xu, 1993*), combustion reactions (*Pina, 1998*) and partial oxidation reactions (*Tellez, 1998; Mallada, 1999*), where alumina, silica and polymeric membranes were used. More recently, a number of studies concerning the use of zeolite membrane reactors (especially MFI-type) have been reported to dehydrogenate i-butane to i-butene (*Coronas and Santamaria, 1999*) by removing selectively the H_2 generated during the reaction from the reaction atmosphere, to distribute O_2 in the oxidative dehydrogenation of propane (*Pantazidis et al., 1995*), and to oxidize butane to maleic anhydride (*Mota et al., 2001*). Hydrophilic zeolite membranes (e.g., mordenite) were used by *Espinoza et al. (1998)* to improve the synthesis of hydrocarbons from synthesis gas by the Fischer-Tropsch process.

On the other hand, zeolite membrane reactors have been also used to carry out liquid-phase reactions where one of the reaction products can be selectively removed by the action of the membrane. In this way, ZSM-5/chabazite/mordenite and zeolite NaA membranes were used by *Salomon et al. (2000)* to produce MTBE from the liquid-phase etherification reaction between *tert*-butanol and methanol catalyzed by acid sulfonic resins by selectively removing part of the water generated during the reaction. Moreover, *Bernal et al. (2000)* and *de la Iglesia et al. (2005)* observed an enhancement of the equilibrium conversion in the liquid-phase esterification reaction of acetic acid with ethanol to produce ethylacetate catalyzed by sulfuric acid when water was selectively removed from the reaction medium by zeolite NaA and mordenite membranes. It should be noted that, compared to mordenite membranes, zeolite NaA membranes suffer from dealumination during the reaction process because of the strong acid conditions. Finally, *Assabumrungrat et al. (2003)* and *Pera-Titus (2001)* simulated a pervaporation membrane reactor to carry out, respectively, the liquid-phase synthesis of ethyl *tert*-butyl ether (ETBE) from the etherification reaction of *tert*-butyl alcohol and ethanol and the liquid-phase synthesis of di-n-pentyl ether (DNPE) from 1-pentanol, being both processes

catalyzed by sulfonated resins. The latter study revealed that 1-pentanol conversion could be enhanced when carried out in a multitubular zeolite NaA membrane reactor compared to a conventional fixed-bed reactor at 423 K and residence time of 35 g h mol^{-1} for the whole reactor.

The latter reaction shows industrial interest because DNPE, a linear and symmetric ether of molecular formula $C_{10}H_{22}O$, shows potential applications as additive in diesel fuels to provide benefits in meeting increasingly stringend diesel exhaust regulations. To reduce such emissions, reformulated fuels are expected to be characterized by higher cetane number, lower density, and lower aromatics, polyaromatics and sulphur contents with respect to the present ones. Using reformulated diesel fuels containing high-quality components may be a good chance to meet such goals. In comparison with short and branched ethers used in gasoline, which have a good octane number but poor cetane number, ethers for diesel have to be linear with a relatively long chain (*Giavazzi et al., 1991; Pecci et al., 1991; Marchionna et al., 1996*). Linear ethers with a chain of nine or more carbon atoms show the best compromise between blending cetane number and blending cold flux properties, which are the most important parameters to assess the quality of a diesel fuel. Among the tested ethers, DNPE turned out to be one of the most promising because it is very effective in reducing emissions (*Van Heerden et al., 1998*) and could be produced industrially form C_4 feedstocks via 1-pentanol, obtained in its turn by selective hydroformylation of linear butenes (oxo process). The details concerning the kinetics of the reaction can be found elsewhere (*Pera-Titus et al., 2001; Cunill et al.,* 2005).